



SAPIENZA
UNIVERSITÀ DI ROMA

PhD Thesis

Sapienza University of Rome
Dottorato di Ricerca in Automatica, Bioingegneria e Ricerca Operativa -
XXXVI Ciclo

Michele Cipriano
ID number 1764645

Advisor
Prof. Giuseppe Oriolo

Academic Year 2023/2024

Thesis defended on TBD May 2024
in front of a Board of Examiners composed by:
Prof. TBD (chairman)
Prof. TBD
Prof. TBD

PhD Thesis
Sapienza University of Rome

© 2024 Michele Cipriano. All rights reserved

This thesis has been typeset by L^AT_EX and the Sapthesis class.

Version: January 24, 2024
Author's email: cipriano@diag.uniroma1.it

Dedication.

Acknowledgments

Acknowledgments.

Abstract

Abstract.

Contents

1	Introduction	1
1.1	Section	1
2	Literature review	2
2.1	Gait generation	2
2.2	Footstep planning	3
2.3	Push recovery for humanoids	4
2.4	Motion control for steerable wheeled mobile robots	4
3	Humanoid motion generation in a world of stairs	5
3.1	Introduction	5
3.1.1	Contribution and paper organization	6
3.2	Problem formulation	7
3.3	The off-line case	9
3.3.1	General architecture	9
3.3.2	Footstep planning	10
3.3.3	Localization	18
3.3.4	Simulations	20
3.4	The on-line case	21
3.4.1	General architecture	22
3.4.2	Mapping	23
3.4.3	Sensor-based footstep planning	24
3.4.4	Visual task generation	26
3.4.5	Simulations	26
3.5	Discussion	29
3.6	Conclusions	30
3.6.1	Pseudocode	31
4	Feasibility-aware plan adaptation in humanoid gait generation	35
4.1	Introduction	35
4.2	Problem formulation	37
4.3	Preliminaries	38
4.3.1	Environment	38
4.3.2	Footstep plan	38
4.4	Gait generation via IS-MPC	39
4.4.1	Prediction model	39

4.4.2	ZMP constraint	40
4.4.3	Stability constraint	41
4.4.4	IS-MPC algorithm	42
4.4.5	Feasibility region	42
4.5	Feasibility-Aware Plan Adaptation	43
4.5.1	Kinematic constraint	44
4.5.2	Timing constraint	44
4.5.3	Patch constraints	44
4.5.4	Current footstep constraints	45
4.5.5	Gait feasibility constraints	46
4.5.6	Feasibility-driven plan adaptation algorithm	46
4.6	Simulations	47
4.7	Conclusions	52
5	Nonlinear model predictive control for steerable wheeled mobile robots	53
6	Conclusions	54
A	Gait generation via IS-MPC	55
A.1	Gait generation via IS-MPC (from WoS)	55
A.1.1	Prediction Model	56
A.1.2	Stability Constraint	56
A.1.3	ZMP Velocity Constraint	58
A.1.4	ZMP Position Constraint	58
A.1.5	QP Problem	61
A.1.6	Proof of Prop. 2	61
B	Real-time nonlinear model predictive control	63

Chapter 1

Introduction

Todo.

1.1 Section

Todo.

Chapter 2

Literature review

Brief intro about literature here.

2.1 Gait generation

Once a footstep sequence has been planned, a whole-body motion must be generated in order to let the robot move by stepping over said sequence without falling. On flat ground, it is common to enforce dynamic balance by requiring that the Zero Moment Point (ZMP, the point with respect to which horizontal components of the momentum of contact forces are zero) is always contained inside the convex hull of contact surfaces, i.e., the *support polygon*. The ZMP cannot be controlled directly, but its dynamics can be related to the position and acceleration of the CoM. The traditional approach is to assume a constant CoM height and a negligible derivative of the angular momentum around the CoM, which leads to a Linear Inverted Pendulum (LIP) [1] model. The LIP has seen widespread use, also thanks to the fact that it allows to perform Model Predictive Control (MPC) using linear-quadratic optimization techniques, enforcing balance by means of constraints on the ZMP. However the constant CoM height assumption limits its ability to be employed for motion on uneven ground.

Traditionally, conditions on the ZMP implicitly assume that the latter is located on the ground, making these conditions obviously unsuitable to the 3D case where there is no univocally defined ground surface. In this work, we adopt an extension [2] of the basic criterion, in which the ZMP is instead a point in 3D space. According to this modified criterion, the 3D ZMP must belong to a pyramidal region whose extent is defined by the position of the Center of Mass (CoM) and the contact surfaces.

By letting the CoM height be a variable quantity, the CoM-ZMP relation takes the form of a Variable Height Inverted Pendulum (VH-IP) [3], where the stiffness of the pendulum itself is a control input. This model is nonlinear, which is usually a problem when trying to perform fast MPC, unless further approximations are introduced. However, it is possible to restrict the allowed trajectories of the CoM in such a way that the dynamics are linear and 3D motions are allowed [4, 5]. To do this, the pendulum stiffness is picked a priori, and the ZMP/CoM trajectories are generated in such a way to satisfy a linear relation.

A common problem in the field of humanoid gait generation is given by the

fact that humanoid dynamics are unstable. This is seen in the LIP by the presence of an unstable mode, and signifies that even if one were to determine a gait such that the ZMP trajectory is always within the appropriate bounds, this might still not be enough, as the associated CoM trajectory might be divergent, rendering the resulting motion infeasible in practice. This issue is crucial and must be accounted for when designing the gait generation module, by providing appropriate guarantees against the divergence of the generated trajectories.

2.2 Footstep planning

Footstep planners can be subdivided in two broad categories based on whether they employ continuous or discrete techniques.

Planners based on continuous techniques compute sequences of footsteps via optimization, treating their poses as continuous decision variables. Several methods in this category (e.g., [6, 7, 8]) rely on the implicit assumption that the ground is completely flat and, therefore, are not tailored for motion generation in 3D environments. Explicit account of 3D environment is instead made in [9]: the ground surface is decomposed as a set of convex regions (with the aid of a manual initialization phase) and footsteps are placed by solving a mixed-integer quadratic problem (MIQP). A more recent work [10] casts the MIQP into a l_1 -minimization problem: to reduce the computational complexity, a suboptimal solution is found by considering only those regions that intersect with the reachable workspace of the feet along a pre-planned trajectory for the floating base of the robot.

Planners based on discrete techniques find a solution by searching among particular sequences of footsteps. These sequences are generated by concatenation of *primitives*. A primitive is a displacement between two consecutive footsteps, selected among a finite number of possible displacements from a catalogue.

To search among all possible sequences, one possibility is to use a deterministic approach, which is typically represented by a variant of A*. Although this is possible and has been applied to 3D environments [11], the approach suffers from two main issues: the performance strongly depends on the chosen heuristic, which is often difficult to design, and node expansion can be very expensive when using a large set of primitives, because it requires the evaluation of all possible successors.

An alternative option is to use a randomized approach such as a variant of the Rapidly-exploring Random Tree (RRT) algorithm. This has been applied in simple 3D environments [12], showing good performance both in planning and replanning for dynamic environments. Clearly the disadvantage of RRT over a deterministic approach is that it does not account, at least in its basic form, for the quality of the footprint plan.

So far, it was assumed that a complete knowledge of the environment is available from the start, or that, in case of dynamic environment, changes to the latter are readily communicated to the planner. However, this is not often the case in practical situations. In fact, the environment could be unknown, either partially or completely, and it must be reconstructed online with the aid of on-board sensors.

Many existing methods exploit information acquired through on-board sensors to identify planar surfaces that define safe regions where the robot can step onto.

Such environment representation was used in combination with different kinds of footstep planners, for example, based on simple geometric criteria [13], A* [14] and MIQP [15]. Other methods maintain a more complete representation of the environment by employing an elevation map. Examples can be found in [16, 17], where ARA*-based approaches are used to plan footsteps on uneven ground; the use of on-line information is aimed at improving the plan during the execution, and not for replanning/extension using newly acquired information. To achieve more flexibility in the on-line capabilities, [18] proposed to use adaptive sets of possible foot displacements in an A*-based planner, which proved to be effective in relatively simple scenarios. Alternatively, [19] proposed a two-stage method that first finds a collision-free path for a bounding occupancy volume and then computes a compatible sequence of footsteps, which is a suitable technique as long as it is not necessary to traverse narrow passages.

2.3 Push recovery for humanoids

Todo.

2.4 Motion control for steerable wheeled mobile robots

Todo.

Chapter 3

Humanoid motion generation in a world of stairs

3.1 Introduction

Humanoid robots, thanks to their ability to perform legged locomotion, are in principle capable of moving through 3D environments, for which complex motions might be required. These can include stepping over or onto obstacles, climbing and descending stairs, moving through surfaces located at different height, overcoming gaps, and so on.

Walking on uneven ground, however, is a challenging task. Management of the footstep locations is subject to several constraints that are completely absent in flat ground locomotion, such as the necessity to avoid placing the feet over the edge of a stair step, or determining whether a given feature of the environment should be considered useful surface onto which the robot can step or simply regarded as an obstacle and avoided altogether.

Also from a control standpoint, walking on uneven ground introduces complications in the dynamic model that are not present in flat ground locomotion. In fact, traditional humanoid locomotion is realized by approximating the dynamics using linear models, which are relatively accurate in many application. Straight up extending these models to 3D environments can lead, without additional considerations, to nonlinearities which can severely impact the performance and theoretical guarantees of the controller.

In this paper we consider the problem of generating a humanoid motion in a *world of stairs*, a specific kind of uneven ground consisting of horizontal patches located at different heights. In order to successfully achieve this, it is necessary to plan a footstep sequence and a whole body motion for the humanoid realizing such sequence. We choose to approach the problem by keeping these two stages separate. The reason for this choice is that in this way we can better control the quality of the produced motions. In fact, the quality of the footstep plan can be evaluated based on global requirements, such as the number of steps taken, or a different performance index. As for the quality of the motion itself, this should be mainly addressed by its capability to satisfy all the required constraints, in order to avoid falls and instabilities. Maintaining a separation between planning and control

also greatly simplifies the tuning because the domain in which any given parameter has effect is reduced.

Keeping planning and control separated is relatively straightforward when the planning is done off-line. However, it might be more difficult to realize if one wants to allow for on-line planning and replanning. In this paper, we will discuss an on-line architecture that achieves this by having short planning stages interleaved with the motion, in such a way that the planning can fully utilize sensor information gathered by the robot as it moves, and that the robot itself can take advantage of the on-line planner to find more efficient and safe footstep sequences.

In the following, we present a review of the state-of-the-art by separating the literature that is more focused on the planning aspect from the literature about gait generation and humanoid robot control. Subsequently, we will describe the contributions of the paper, focusing on the improvements with respect to the state-of-the-art.

3.1.1 Contribution and paper organization

In this paper, we consider planning both in off-line situations, in which the environment is completely known, and on-line situations, in which the geometry of the environment is not known in advance and must be reconstructed by the robot itself during motion using on-board sensors. In this case, planning and execution are interdependent: the former clearly requires the latter in order to determine where to place the footsteps, but the converse is also true, as the real-time motion of the robot is necessary to acquire information about the environment.

With respect to the previously reviewed contributions, our work improves the following points:

- the proposed footstep planner finds sequences of footsteps that are optimal with respect to a chosen optimality criterion, whereas most of the literature that makes use of randomized methods does not in any way consider the quality of the produced sequences [12]; we do this by using a planner based on RRT*, which is a probabilistic method with guarantees of asymptotic convergence to an optimal solution;
- in our formulation, optimality does not significantly compromise performance, unlike techniques that make use of A*-based algorithms [14, 16, 18], or others that make use of quadratic optimization [9];
- we propose a scheme capable of working both with off-line planning, in known environments, and in on-line situations;
- to generate a gait that realizes the footstep plan we adopt and improve our Intrinsically Stable MPC (IS-MPC) scheme [20]. IS-MPC incorporates an explicit stability constraint in order to deal with the instability in the humanoid robot dynamics. Along with the stability constraint, we enforce a ZMP position constraint and a ZMP velocity constraint, and show that the combination of all the imposed constraints guarantees satisfaction of the balance condition in 3D.

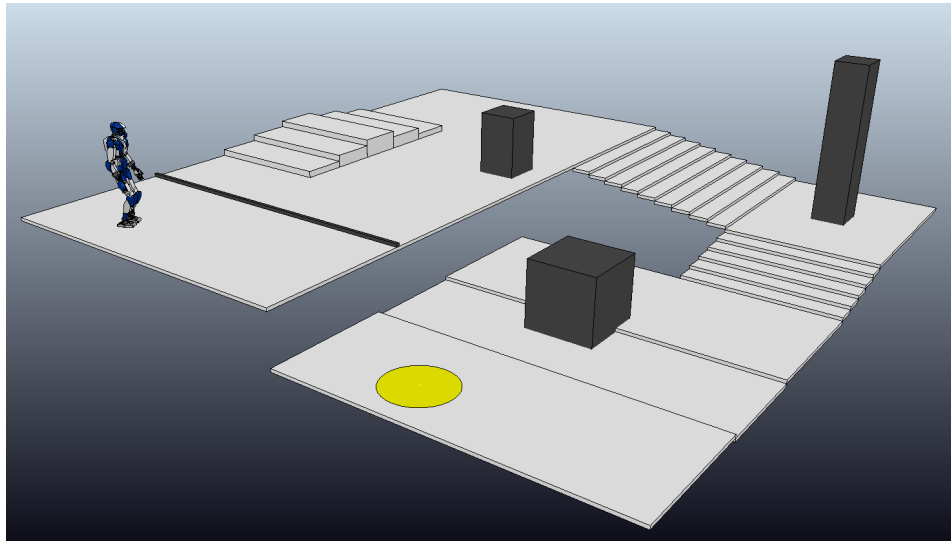


Figure 3.1. An instance of the considered problem. The robot must reach the goal region (in yellow) by traversing a *world of stairs*. Patches that are not visible correspond to infinitely deep holes or trenches.

Compared to our previous work on the subject, [5], the main additions presented in this paper consist of the introduction of optimality criteria in the planner, the extension to on-line situations with the use of on-board sensors, and the inclusion of the ZMP velocity constraint in the IS-MPC. We validate the proposed architectures for the off-line and on-line case via simulations on the HRP-4 humanoid robot in scenarios of different complexity.

The paper is structured as follows. Section 3.2 formulates the problem both in the off-line and in the on-line case. Section 3.3 presents in detail the off-line case by discussing its general architecture in Sect. 3.3.1, describing the footstep planner and the scenarios used for testing in Sect. 3.3.2, the gait generation module together with theoretical developments in Sect. A.1, the localization module in Sect. 3.3.3 and the simulations in Sect. 3.3.4. Section 3.4 extends the work to the on-line case, presenting its architecture in Sect. 3.4.1, the mapping module in Sect. 3.4.2, the sensor-based footstep planner in Sect. 3.4.3, the visual task generation module in Sect. 3.4.4 and simulations in both static and dynamic environments in Sect. 3.4.5. Section 3.5 puts the paper in perspective with respect to the state of the art, and Sect. 3.6 concludes the paper with mentions to possible future work.

3.2 Problem formulation

In the situation of interest (Fig. 3.1), a humanoid robot moves in a *world of stairs*, a specific kind of uneven ground consisting of horizontal patches that (*i*) are located at different heights, and (*ii*) constitute a partition¹ of \mathbb{R}^2 . Depending on its elevation with respect to the neighboring areas, a patch may be accessible for the humanoid to climb on from an appropriate direction; otherwise, it actually represents an *obstacle*

¹This implies that the whole volume of space below any horizontal patch is occupied.

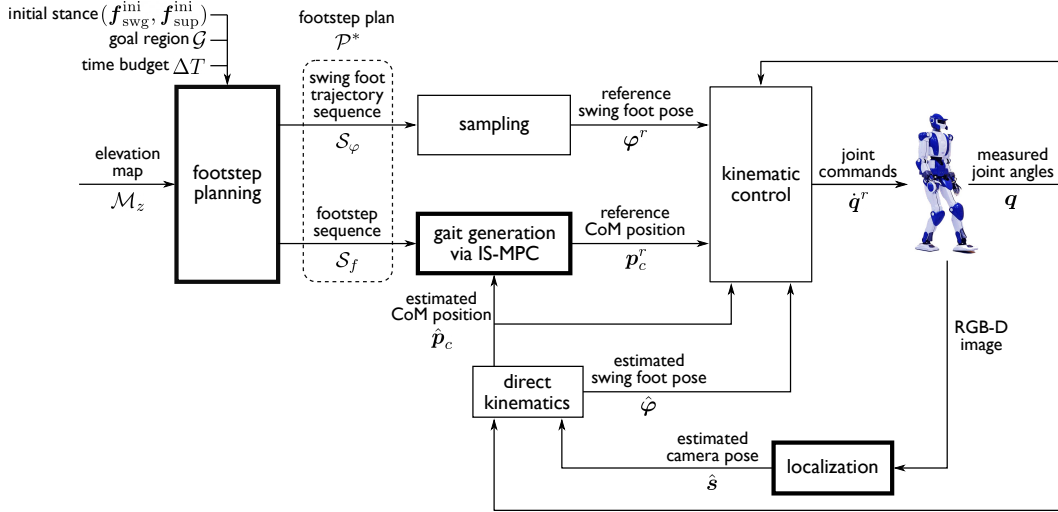


Figure 3.2. Block scheme of the proposed solution approach for the off-line case.

to be avoided. Any accessible patch may be stepped on, stepped over or even circumvented, depending on the generated motion.

The mission of the robot is to reach a certain goal region \mathcal{G} , which will belong in general to a single patch (Fig. 3.1). In particular, this locomotion task is accomplished as soon as the robot places a footstep inside \mathcal{G} .

We want to devise a complete framework enabling the humanoid to plan and execute a motion to fulfill the assigned task in the world of stairs. This requires addressing two fundamental problems: finding a 3D footstep plan and generating a variable-height gait that is consistent with such plan. Footstep planning consists in finding both footstep placements and swing foot trajectories between them; overall, the footstep plan must be feasible (in a sense to be formally defined later) for the humanoid, given the characteristics of the environment. Gait generation consists in finding a CoM trajectory which realizes the footstep plan while guaranteeing dynamic balance of the robot at all time instants. From the trajectories of the CoM and the feet, a whole-body motion may be computed using inverse kinematics methods.

In particular, we will address two versions of the above problem, henceforth referred to as the *off-line* and *on-line* case. In the first, the geometry of the environment is completely known in advance, while in the second it is reconstructed by the robot itself as it moves. In the following we describe the architectures designed for the off-line and on-line case supposing that the environment is static. However, we will also show that the latter can be used effectively in dynamic environments, thanks to its fast replanning capabilities.

The problem will be solved under the following assumptions.

- A1 Information about the environment is maintained in an *elevation map* M_z , i.e., a 2.5D grid map of equally-sized cells that, whenever needed, can be queried as $z = M_z(x, y)$, to provide the height of the ground at the cell having coordinates (x, y) [21]. In the off-line case, M_z is available a priori, while in the on-line case it must be incrementally built by the humanoid based on

sensory information.

- A2 The humanoid is equipped with a head-mounted RGB-D camera, which is used for localization in both the off-line and on-line cases, and also updating the elevation map \mathcal{M}_z in the latter.
- A3 The humanoid is endowed with a localization module which provides an estimate of the camera pose at each time instant, based on information gathered by the RGB-D camera. This is used in both the off-line and on-line cases.
- A4 The friction between the robot feet and the ground is sufficiently large to avoid slipping at the contact surfaces².

In the off-line case, a complete footstep plan leading to the goal region \mathcal{G} will be computed before the humanoid starts to move. In the on-line case, the footstep plan will instead be updated during motion, based on new information added to \mathcal{M}_z .

In the following, we first address in full detail the off-line case and then proceed to extending the proposed approach to the on-line case.

3.3 The off-line case

We start this section by describing the general structure of the proposed method. Then we will describe in detail its main components, i.e., the footstep planner and the gait generation scheme based on IS-MPC. Some simulation results will also be presented.

3.3.1 General architecture

To solve the described problem in the off-line case, we adopt the architecture shown in Fig. 3.2, in which the main components are the footstep planning, gait generation and localization modules.

In the following, we denote by $\mathbf{f} = (x_f, y_f, z_f, \theta_f)$ the *pose* of a certain footstep, with x_f , y_f , z_f representing the coordinates of a representative point, henceforth collectively denoted as \mathbf{p}_f , and θ_f its orientation³. Moreover, a pair $(\mathbf{f}_{\text{swg}}, \mathbf{f}_{\text{sup}})$ defines a *stance*, i.e., the feet poses during a double support phase after which a step is performed by moving the swing foot from \mathbf{f}_{swg} while keeping the support foot at \mathbf{f}_{sup} .

The footstep planner receives in input the initial humanoid stance⁴ $(\mathbf{f}_{\text{swg}}^{\text{ini}}, \mathbf{f}_{\text{sup}}^{\text{ini}})$ at $t = 0$, the goal region \mathcal{G} , a time budget ΔT , and the elevation map \mathcal{M}_z representing the environment.

²Since our objective is to generate walking gaits in a world of stairs, we expect that the horizontal components of the ground reaction forces will be rather limited with respect to the vertical components, making this assumption reasonable. To support this claim, we explicitly verified that Assumption A4 holds in our simulations, see the related comment toward the end of Sect. 3.3.4. Nevertheless, the constraint that ground reaction forces must always be contained in the friction cone can be incorporated in our formulation; this extension would be required in the case of non-horizontal contact surfaces.

³To represent the footstep orientation we only use the yaw angle, as roll and pitch are always zero thanks to the piecewise-horizontal ground assumption.

⁴The initial support foot can be chosen arbitrarily.

The time budget represents the time given to the planner to find a solution. When this time runs over, the algorithm either returns a solution or ends with a failure. Explicitly specifying this time as input to the algorithm allows us to evaluate the performance of the planning module, but also proves to be useful for the extension to the on-line case, where the time budget is set equal to the duration of a step in order to meet the real-time requirement.

The planner works off-line to find, within ΔT , an optimal *footstep plan* $\mathcal{P}^* = \{\mathcal{S}_f, \mathcal{S}_\varphi\}$ leading to the desired goal region \mathcal{G} . In \mathcal{P}^* , we denote by

$$\mathcal{S}_f = \{\mathbf{f}^1, \dots, \mathbf{f}^n\}$$

the sequence of footstep placements, whose generic element \mathbf{f}^j is the pose of the j -th footstep, with $\mathbf{f}^1 = \mathbf{f}_{\text{swg}}^{\text{ini}}$ and $\mathbf{f}^2 = \mathbf{f}_{\text{sup}}^{\text{ini}}$. Also, we denote by

$$\mathcal{S}_\varphi = \{\boldsymbol{\varphi}^1, \dots, \boldsymbol{\varphi}^{n-2}\}$$

the sequence of associated swing foot trajectories, whose generic element $\boldsymbol{\varphi}^j$ is the j -th *step*, i.e., the trajectory leading the foot from \mathbf{f}^j to \mathbf{f}^{j+2} . Its duration T_s^j is split in T_{ss}^j and T_{ds}^j , respectively the single and double support phases. The timestamp of a generic footstep indicates the beginning of the j -th step, i.e., of the j -th single support phase; thus, \mathbf{f}^j has an associated timestamp $t_s^j = t_s^{j-1} + T_s^{j-1}$, with $t_s^1 = 0$.

Once the footstep plan has been generated, the sequence of footsteps \mathcal{S}_f is sent to a gait generator based on Intrinsically Stable MPC (IS-MPC), which computes in real time a variable-height CoM trajectory that is compatible with \mathcal{S}_f and guaranteed to be *stable* (i.e., bounded with respect to the ZMP). In particular, we denote by \mathbf{p}_c^r the current reference position of the CoM produced by IS-MPC. Also, let $\boldsymbol{\varphi}^r$ be the current reference pose of the swing foot, obtained by sampling the appropriate subtrajectory in \mathcal{S}_φ . Then, \mathbf{p}_c^r and $\boldsymbol{\varphi}^r$ are passed to a kinematic controller which computes the joint commands $\dot{\mathbf{q}}^r$ for the robot.

Visual information, gathered by the head-mounted camera in the form of RGB-D images, is provided to the localization module, which continuously updates the estimate $\hat{\mathbf{s}}$ of the pose of the camera frame. From this, and using joint encoder data, it is possible to obtain estimates for the CoM position and swing foot pose ($\hat{\mathbf{p}}_c$ and $\hat{\boldsymbol{\varphi}}$, respectively) through kinematic computations. Finally, these estimates are used to provide feedback to both the gait generation and kinematic control modules.

3.3.2 Footstep planning

The input data for this module are the initial robot stance ($\mathbf{f}_{\text{swg}}^{\text{ini}}, \mathbf{f}_{\text{sup}}^{\text{ini}}$), the goal region \mathcal{G} , the time budget ΔT and the elevation map \mathcal{M}_z . Given an optimality criterion, the footstep planner returns the best footstep plan \mathcal{P}^* leading to \mathcal{G} found within ΔT .

The planning algorithm builds a tree \mathcal{T} , where each vertex $v = (\mathbf{f}_{\text{swg}}, \mathbf{f}_{\text{sup}})$ specifies a stance, and an edge between two vertexes v and $v' = (\mathbf{f}'_{\text{swg}} = \mathbf{f}_{\text{sup}}, \mathbf{f}'_{\text{sup}})$ indicates a step between the two stances, i.e., a collision-free trajectory such that one foot swings from \mathbf{f}_{swg} to \mathbf{f}'_{sup} and the other is fixed at \mathbf{f}_{sup} .

The expansion process makes use of a catalogue U of *primitives*, which allows to generate new footsteps by selecting them from a finite set of displacements with

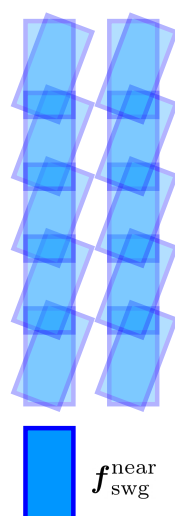
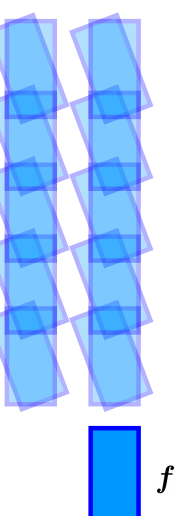
catalogue U	
left support	right support
	

Figure 3.3. An example catalogue U of primitives, containing a finite set of landings for the swing foot with respect to the left or right support foot.

respect to the support foot. The catalogue is split in two subsets, one for the case of left support and the other for the case of right support; at each instant, the appropriate subset is used. An example catalogue is shown in Fig. 3.3.

Each branch joining the root of the tree to a generic vertex v represents a footstep plan \mathcal{P} . The sequences \mathcal{S}_f and \mathcal{S}_φ for this plan are respectively obtained by taking along the branch the support foot poses of all vertexes and the steps corresponding to all edges.

Footstep feasibility

Footstep $\mathbf{f}^j = (x_f^j, y_f^j, z_f^j, \theta_f^j) \in \mathcal{S}_f$ is *feasible* if it satisfies the following requirements:

R1 \mathbf{f}^j is fully in contact within a single horizontal patch.

To guarantee this, each cell of \mathcal{M}_z belonging to, or overlapping with, the footprint at \mathbf{f}^j must have the same height z_f^j . In practice, one typically uses an enlarged footprint to ensure that this requirement will still be satisfied in the presence of small positioning errors.

R2 \mathbf{f}^j is kinematically admissible from the previous footstep \mathbf{f}^{j-1} (this is actually *stance feasibility*).

The admissible region (a submanifold of $\mathbb{R}^3 \times SO(2)$) for placing \mathbf{f}^j next to

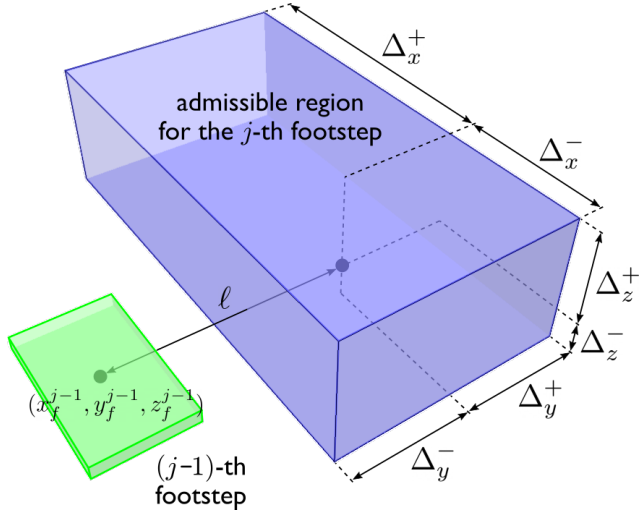


Figure 3.4. The 3D admissible region identified by the first two kinematic constraints of requirement R2, i.e., eqs. (3.1–3.2). Footstep orientation is not represented.

\mathbf{f}^{j-1} is defined by the following constraints:

$$-\begin{pmatrix} \Delta_x^- \\ \Delta_y^- \end{pmatrix} \leq R_{j-1}^T \begin{pmatrix} x_f^j - x_f^{j-1} \\ y_f^j - y_f^{j-1} \end{pmatrix} \pm \begin{pmatrix} 0 \\ \ell \end{pmatrix} \leq \begin{pmatrix} \Delta_x^+ \\ \Delta_y^+ \end{pmatrix} \quad (3.1)$$

$$-\Delta_z^- \leq z_f^j - z_f^{j-1} \leq \Delta_z^+ \quad (3.2)$$

$$-\Delta_\theta^- \leq \theta_f^j - \theta_f^{j-1} \leq \Delta_\theta^+. \quad (3.3)$$

Here, R_{j-1} is the planar rotation matrix associated with θ_f^{j-1} and the Δ symbols are lower and upper maximum increments, see Fig. 3.4.

R3 \mathbf{f}^j is reachable from \mathbf{f}^{j-2} through a collision-free motion (this is actually *step feasibility*).

Since information about the whole-body motion of the robot is not yet available during footstep planning (it will only be defined in the subsequent gait generation phase), this requirement can only be tested conservatively. In particular, we say that R3 is satisfied if (i) there exist a collision-free swing foot trajectory φ^{j-2} from \mathbf{f}^{j-2} to \mathbf{f}^j generated by the engine of Sect. 3.3.2, and (ii) a suitable volume \mathcal{B} accounting for the maximum occupancy of the humanoid upper body at stance $(\mathbf{f}^{j-1}, \mathbf{f}^j)$ is collision-free. More precisely, \mathcal{B} is a vertical cylinder whose base has radius r_b and center at $(x_m, y_m, z_m + z_b)$, where x_m , y_m , z_m are the coordinates of the midpoint \mathbf{m} between the footsteps and z_b is a vertical offset representing the average distance between the ground and the hip (Fig. 3.5). Note that any nonzero height can be used for the cylinder in view of the world of stairs assumption, which implies that \mathcal{B} is collision-free⁵

⁵Even though the volume for checking the upper body collision is chosen conservatively, this does not guarantee obstacle avoidance because the lower body is not considered. However, whole-body

if each cell of \mathcal{M}_z belonging to, or overlapping with, its ground projection has height smaller than $z_m + z_b$.

Vertex identity, neighbors and cost

The *identity* of a vertex $v = (\mathbf{f}_{\text{swg}}, \mathbf{f}_{\text{sup}})$ indicates whether \mathbf{f}_{swg} refers to the left (L) or the right (R) foot:

$$\text{id}(v) = \begin{cases} L & \text{if } \text{id}(v^{\text{parent}}) = R \\ R & \text{if } \text{id}(v^{\text{parent}}) = L, \end{cases}$$

where v^{parent} is the parent vertex of v . This definition determines the identity of each vertex, once the identity of the root is assigned.

We also define the set of *neighbors* of $v = (\mathbf{f}_{\text{swg}}, \mathbf{f}_{\text{sup}})$

$$\mathcal{N}(v) = \{v' = (\mathbf{f}'_{\text{swg}}, \mathbf{f}'_{\text{sup}}) \in \mathcal{T} : \gamma(\mathbf{f}_{\text{sup}}, \mathbf{f}'_{\text{sup}}) \leq r_{\text{neigh}}\}$$

where r_{neigh} is a threshold distance and

$$\gamma(\mathbf{f}, \mathbf{f}') = \|\mathbf{p}_f - \mathbf{p}'_f\| + k_\gamma |\theta_f - \theta'_f| \quad (3.4)$$

is a footstep-to-footstep metric, with $k_\gamma \geq 0$.

Assume that the edge between two vertexes v^a and v^b of \mathcal{T} has a cost $l(v^a, v^b)$. The *cost* of a vertex v is defined as

$$c(v) = c(v^{\text{parent}}) + l(v^{\text{parent}}, v)$$

and represents the cost of reaching v from the root of \mathcal{T} . Then, the cost of a plan \mathcal{P} ending at a vertex v is $c(\mathcal{P}) = c(v)$.

In particular, we will consider three possibilities for the cost of an edge. The first is

$$l_1(v^a, v^b) = 1, \quad (3.5)$$

for all edges in \mathcal{T} . The corresponding vertex cost will be denoted by $c_1(v)$ and represents the length of the corresponding plan in terms of number of edges (i.e., steps).

The second edge cost represents the net height variation of the swing foot during a step:

$$l_2(v^a, v^b) = |z_{f,\text{sup}}^b - z_{f,\text{swg}}^a|, \quad (3.6)$$

where $z_{f,\text{swg}}^a$ and $z_{f,\text{sup}}^b$ are the z -component of, respectively, the swing foot at v^a and the support foot at v^b . The corresponding vertex cost will be denoted by $c_2(v)$ and represents the cumulative height variation along the corresponding plan.

Finally, we also consider an edge cost

$$l_3(v^a, v^b) = \frac{1}{\sigma(\mathbf{f}_{\text{sup}}^b)}, \quad (3.7)$$

collision avoidance can be obtained by including appropriate constraints in the kinematic controller [22].

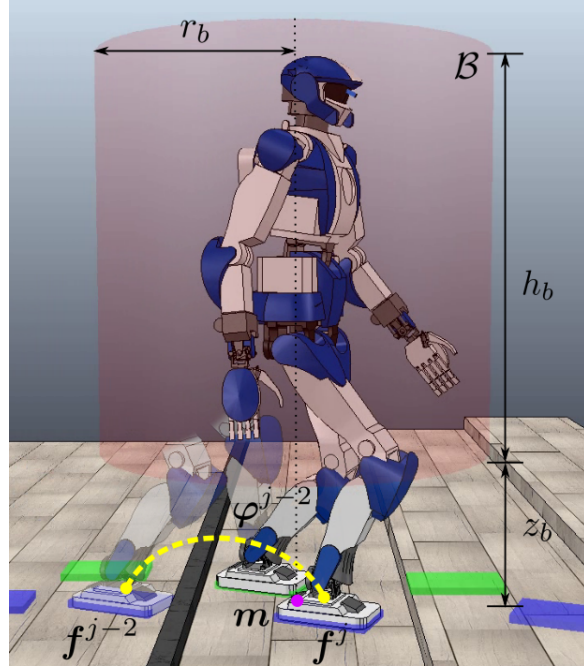


Figure 3.5. Visual representation of the process for checking requirement R3. The red cylinder accounts for the maximum occupancy of the humanoid upper body, while the yellow line represents the swing foot trajectory.

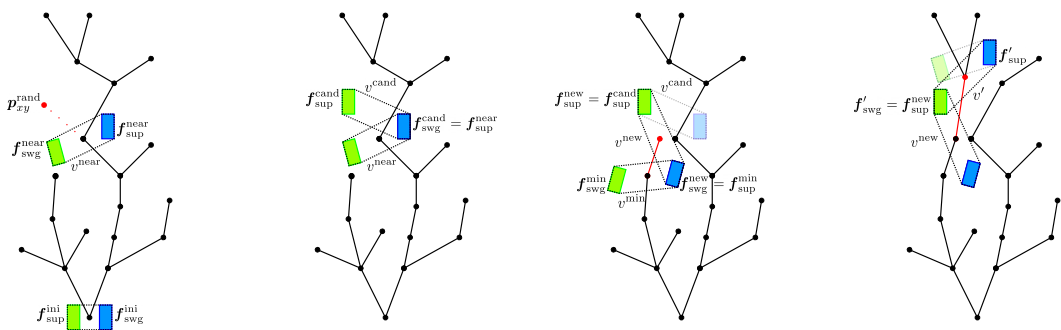


Figure 3.6. The four steps of a generic iteration of the footstep planner. From left to right: selecting a vertex for expansion, generating a candidate vertex, choosing a parent, rewiring.

where $\sigma(\mathbf{f}_{\text{sup}}^b)$ is the *clearance* of the support foot $\mathbf{f}_{\text{sup}}^b$ at v^b , defined as the distance between the representative point of $\mathbf{f}_{\text{sup}}^b$ and the closest point in \mathcal{M}_z w.r.t. which the absolute height variation is larger than $\max\{\Delta_z^-, \Delta_z^+\}$ ⁶. This cost penalizes steps that bring the swing foot too close to a drop or to a vertical surface leading to a contiguous higher patch, while still allowing to approach accessible patches such as staircases. The corresponding vertex cost, denoted by $c_3(v)$, represents the cumulative inverse clearance along the corresponding plan.

Other kinds of cost functions can be considered. For example, one could penalize unnecessary rotations of the next footstep with respect to the support footstep in order to obtain smoother plans. In general, it may be advisable to use a weighted combination of several optimality criteria for better practical performance.

Algorithm

At the beginning, \mathcal{T} is rooted at $(\mathbf{f}_{\text{swg}}^{\text{ini}}, \mathbf{f}_{\text{sup}}^{\text{ini}})$, the initial stance of the humanoid. Then, \mathcal{T} is expanded using an RRT*-like strategy. The generic iteration consists of: selecting a vertex for expansion, generating a candidate vertex, choosing a parent for the new vertex and rewiring the tree. These individual steps are described in the following, see also Fig. 3.6.

Selecting a vertex for expansion: A point $\mathbf{p}_{xy}^{\text{rand}}$ is randomly selected on the xy -plane, and the vertex v^{near} that is closest to $\mathbf{p}_{xy}^{\text{rand}}$ is identified. To this end, we define a vertex-to-point metric as

$$\mu(v, \mathbf{p}_{xy}) = \|\mathbf{m}_{xy}(v) - \mathbf{p}_{xy}\| + k_\mu |\psi(v, \mathbf{p}_{xy})|,$$

where $\mathbf{m}_{xy}(v)$ represents the planar position of the midpoint between the feet at stance v , k_μ is a positive scalar, and $\psi(v, \mathbf{p}_{xy})$ is the angle between the robot sagittal axis (whose orientation is the average of the orientations of the two footsteps) and the line joining \mathbf{m}_{xy} to \mathbf{p}_{xy} . ◀

Generating a candidate vertex: After identifying the vertex $v^{\text{near}} = (\mathbf{f}_{\text{swg}}^{\text{near}}, \mathbf{f}_{\text{sup}}^{\text{near}})$, a candidate footstep is first generated using the catalogue U (see Fig. 3.3). In particular, we set the support foot to $\mathbf{f}_{\text{sup}}^{\text{near}}$ and randomly select one element from the subset of U associated to the identity of v^{near} , which may be L (left) or R (right). Note that all elements of U are chosen so as to automatically satisfy conditions (3.1–3.3) of requirement R2. Call $\mathbf{f}_{\text{sup}}^{\text{cand}}$ the chosen candidate footstep. The z coordinate to be associated to the footstep $\mathbf{f}_{\text{sup}}^{\text{cand}}$ is then retrieved from \mathcal{M}_z , and both the requirement R1 and the last condition (3.2) of R2 can now be checked.

To test the last requirement R3, we invoke an engine that generates a swing foot trajectory φ^{near} from $\mathbf{f}_{\text{swg}}^{\text{near}}$ to $\mathbf{f}_{\text{sup}}^{\text{cand}}$. Such engine uses a parameterized trajectory which, given the endpoints, can be deformed⁷ by varying the maximum height h along the motion. Using the elevation map and increments of Δh , the engine tries growing values of h in a certain range $[h^{\min}, h^{\max}]$ looking for a collision-free trajectory.

⁶This information may be precomputed from the elevation map \mathcal{M}_z and stored in a clearance map.

⁷As a deformable trajectory we used a polynomial, but other choices (e.g., B-splines and Bezier curves) are possible.

If all requirements have been satisfied, a candidate vertex is generated as $v^{\text{cand}} = (\mathbf{f}_{\text{swg}}^{\text{cand}}, \mathbf{f}_{\text{sup}}^{\text{cand}})$, with $\mathbf{f}_{\text{swg}}^{\text{cand}} = \mathbf{f}_{\text{sup}}^{\text{near}}$; however, v^{cand} is not added to \mathcal{T} because the planner first needs to identify the best parent for it. If any requirement among R1–R3 is violated, the current expansion attempt is aborted and a new iteration is started. \blacktriangleleft

Choosing a parent: Although v^{cand} was generated from v^{near} , there might be a different vertex in the tree that leads to the same vertex with a lower cost. To find it, the planner checks for each vertex $v' = (\mathbf{f}'_{\text{swg}}, \mathbf{f}'_{\text{sup}}) \in \mathcal{N}(v^{\text{cand}})$ whether setting v' as parent of v^{cand} satisfies requirements R2–R3, and whether this connection reduces the cost of v^{cand} , that is

$$c(v') + l(v', v^{\text{cand}}) < c(v^{\text{near}}) + l(v^{\text{near}}, v^{\text{cand}}).$$

The vertex $v^{\text{min}} = (\mathbf{f}_{\text{swg}}^{\text{min}}, \mathbf{f}_{\text{sup}}^{\text{min}})$ that allows to reach v^{cand} with minimum cost is chosen as its parent. If $v^{\text{min}} = v^{\text{near}}$, then v^{cand} can be added to the tree together with the edge joining it to v^{near} . However, if a different parent $v^{\text{min}} \neq v^{\text{near}}$ is chosen, the candidate vertex v^{cand} must be modified by relocating its swing footstep to the support footstep of v^{min} . To this end, a new vertex $v^{\text{new}} = (\mathbf{f}_{\text{swg}}^{\text{new}}, \mathbf{f}_{\text{sup}}^{\text{new}})$ with $\mathbf{f}_{\text{swg}}^{\text{new}} = \mathbf{f}_{\text{sup}}^{\text{min}}$ and $\mathbf{f}_{\text{sup}}^{\text{new}} = \mathbf{f}_{\text{sup}}^{\text{cand}}$ is generated and added to \mathcal{T} as child of v^{min} . The edge between v^{min} and v^{new} corresponds to the swing foot trajectory φ^{min} . \blacktriangleleft

Rewiring: This final step checks whether v^{new} allows to reach with a lower cost some vertex already in \mathcal{T} , and updates the tree accordingly. In particular, for each $v' = (\mathbf{f}'_{\text{swg}}, \mathbf{f}'_{\text{sup}}) \in \mathcal{N}(v^{\text{new}})$, the procedure checks whether setting v' as a child of v^{new} satisfies requirements R2–R3, and whether this connection reduces the cost of v' , that is

$$c(v^{\text{new}}) + l(v^{\text{new}}, v') < c(v').$$

If this is the case, v' is modified (similarly to what was done when choosing a parent) by relocating its swing footstep to $\mathbf{f}_{\text{sup}}^{\text{new}}$, and then reconnected to \mathcal{T} as a child of v^{new} . The edge between v^{new} and v' corresponds to the swing foot trajectory φ^{new} . Finally, for each child $v'' = (\mathbf{f}''_{\text{swg}}, \mathbf{f}''_{\text{sup}})$ of v' , the swing foot trajectory φ' from the relocated \mathbf{f}'_{swg} to $\mathbf{f}''_{\text{sup}}$ is generated and the edge between v' and v'' is accordingly updated⁸.

Note that, although $\mathcal{N}(v^{\text{new}})$ can contain ancestors of v^{new} , no cycle will be generated by rewiring. In fact, it can be easily shown that any ancestor of v^{new} will have a cost lower or equal than $c(v^{\text{new}})$, so that it will never be set as its child. \blacktriangleleft

When the assigned time budget ΔT runs out, tree expansion is stopped. The set $\mathcal{V}_{\text{goal}}$ of vertexes v such that $\mathbf{p}_{f,\text{sup}} \in \mathcal{G}$ is retrieved. The vertex v^* with minimum cost is selected as

$$v^* = \underset{v \in \mathcal{V}_{\text{goal}}}{\operatorname{argmin}} c(v) \tag{3.8}$$

and the corresponding footstep plan \mathcal{P}^* is retrieved from the branch of \mathcal{T} joining the root to v^* .

Clearly, the larger the time budget, the better the quality of the obtained footstep plan. We conjecture that our planner inherits the asymptotic optimality property of the general RRT* algorithm [23], although we do not have a formal proof yet.

⁸In case the engine fails to find such trajectory, the subtree rooted at vertex v'' (including v'' itself) is simply removed from \mathcal{T} .



Figure 3.7. The considered scenarios, from left to right: *Rod*, *Ditch*, *Corridor*, *Maze*, *Spacious*.

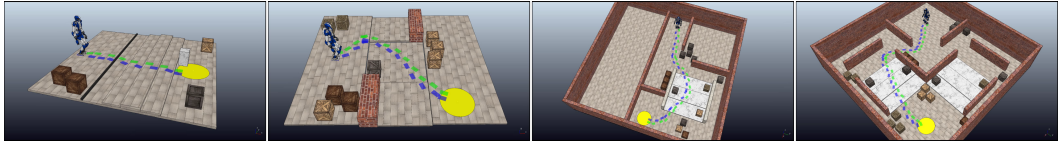


Figure 3.8. Examples of footstep plans found in the scenarios *Rod*, *Ditch*, *Corridor* and *Maze*, respectively, when minimizing the number of steps.

Planning Results

To assess the performance of the proposed footstep planner, we performed a campaign of planning experiments through our C++ implementation on an Intel Core i7-8700K CPU running at 3.7 GHz. The tree constructed by the planner is stored in a k-d tree structure [24], which allows to efficiently perform search and insertion operations. The used robot is HRP-4, a 1.5 m tall humanoid with 34 degrees of freedom by Kawada Robotics.

We considered the five different scenarios (see Fig. 3.7) of different complexity described in the following.

- *Rod*. A thin straight obstacle, which does not provide a large enough surface to step on, must be overcome before ascending and descending a staircase.
- *Ditch*. A ditch can only be entered from the left and exited from the right, because the platform in the middle of it is too low to be accessed directly.
- *Corridor*. A corridor must be exited before ascending and descending a staircase.
- *Maze*. A maze must be navigated, including ascending and descending a staircase, to reach the goal region.
- *Spacious*. The goal region can be reached either by traversing a flat ground or ascending and descending a staircase.

The height of each step is 8 cm for all scenarios except *Ditch* where the height is 10 cm.

In all scenarios, the robot has to reach a circular goal region of radius 0.5 m. The catalogue of primitives U is generated by listing all possible combinations of the following parameters: longitudinal displacement $\{-0.08, 0.00, 0.08, 0.16, 0.2\}$ [m], lateral displacement $\{0.20, 0.30\}$ [m] for right support and $\{-0.20, -0.30\}$ [m] for left support, angular displacement $\{0.00, 0.40\}$ [rad] for right support and $\{0.00, -0.40\}$ [rad] for left support (see Fig. 3.3). In the off-line footstep planner we have set $k_\mu = 1$, $k_\gamma = 0$, $h_{\min} = 0.02$ m, $h_{\max} = 0.24$ m, $\Delta h = 0.02$ m, $\Delta_x^- = 0.08$ m, $\Delta_x^+ = 0.24$ m,

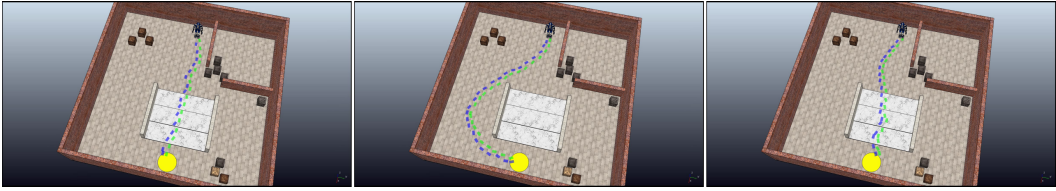


Figure 3.9. Examples of footstep plans found in the scenario *Spacious* when minimizing the number of steps, minimizing the height variation and maximizing the clearance, respectively.

$\Delta_y^- = 0.07$ m, $\Delta_y^+ = 0.07$ m, $\Delta_z^- = 0.16$ m, $\Delta_z^+ = 0.16$ m, $\Delta_\theta^- = 0.3$ rad, $\Delta_\theta^+ = 0.3$ rad, $\ell = 0.25$ m, $z_b = 0.3$ m, $h_b = 1.2$ m, and $r_b = 0.25$ m. The elevation map \mathcal{M}_z has a resolution of 0.02 m. The three quality criteria described in Sect. 3.3.2 are considered in each scenario.

Tables 3.1–3.3 show the performance of the planner in each scenario, for different values of the time budget, when choosing the three optimality criteria described in Sect. 3.3.2, respectively. In each table, each row reports the results obtained over 100 runs on a combination of scenario and time budget. A total of six performance indexes are tracked and averaged over the total number of successful runs. In particular, a run is considered unsuccessful if the planner terminates without placing any footstep in the goal region. Note that all unsuccessful cases are due to inappropriate time budget. Examination of the table confirms that increasing the time budget both solves this problem by ensuring a high success rate, and improves the quality of the plan in terms of the average cost (Avg Cost). This result supports our conjecture about the asymptotic optimality of the proposed footstep planner.

Figure 3.8 shows the plans generated by minimizing the number of steps in the scenarios *Rod*, *Ditch*, *Corridor* and *Maze*. In particular, in *Rod* the plan allows to correctly pass over the thin obstacle and walk the stairway, eventually reaching the goal region; in *Ditch* the plan reaches the left patch before traversing the low central patches; in *Corridor* the plan manages to exit the first room, reaching the stairway and avoiding the obstacles; in *Maze* the plan takes the left path among the two available, which is the optimal one. Figure 3.9 compares the plans generated in the scenario *Spacious* for each considered cost function. In particular, when minimizing the number of steps the plan goes straight towards the goal region; when minimizing the height variation, the plan avoids the stairway; when maximizing the clearance the plan first moves away from the wall placed on the left flank of the robot at its starting configuration, and then moves towards the goal region while keeping the other obstacles at a safe distance.

3.3.3 Localization

The localization module is continuously fed with the RGB-D images gathered by the head-mounted camera. Based on such information, it is in charge of updating in real time the estimate \hat{s} of the pose of the camera frame. To this end, it uses RTAB-Map [25], an open source visual SLAM library. In particular, the visual odometry and graph optimization tool are employed. The first tracks the features automatically extracted from the RGB-D images, while the second minimizes the odometry error

Scenario	Time Budget [s]	Avg Cost	Min Cost	Max Cost	Iters	Tree Size	Successes
<i>Rod</i>	1	22.938	15.000	35.000	6393.8	2948.7	96/100
	5	19.810	15.000	28.000	21537.8	9863.0	100/100
	10	18.050	15.000	25.000	34758.2	15705.5	100/100
	25	16.600	15.000	24.000	62862.0	27944.5	100/100
<i>Ditch</i>	1	40.364	30.000	51.000	5966.7	2119.5	33/100
	5	36.450	27.000	47.000	18632.4	7100.4	100/100
	10	33.420	25.000	42.000	29195.2	11503.3	100/100
	25	30.940	25.000	38.000	52090.5	20755.6	100/100
<i>Corridor</i>	1	57.823	51.000	68.000	6131.4	1880.7	17/100
	5	60.213	46.000	86.000	21589.9	5068.1	89/100
	10	55.687	42.000	81.000	36426.8	8068.1	99/100
	25	49.700	42.000	60.000	70242.7	14415.3	100/100
<i>Maze</i>	1	74.773	62.000	89.000	5813.2	2264.9	22/100
	5	70.949	54.000	94.000	21482.0	8695.5	99/100
	10	65.520	53.000	80.000	35986.2	15327.2	100/100
	25	58.240	50.000	76.000	67507.5	28891.7	100/100
<i>Spacious</i>	1	47.156	37.000	68.000	5749.5	2971.2	96/100
	5	41.700	35.000	55.000	20899.7	10630.8	100/100
	10	39.290	33.000	55.000	34665.6	17412.8	100/100
	25	36.570	31.000	46.000	65308.0	31889.3	100/100

Table 3.1. Performance of the off-line footstep planner when minimizing the number of steps.

Scenario	Time Budget [s]	Avg Cost	Min Cost	Max Cost	Iters	Tree Size	Successes
<i>Rod</i>	1	0.450	0.420	0.480	6634.0	3186.5	96/100
	5	0.431	0.420	0.480	20559.8	9883.2	100/100
	10	0.425	0.420	0.480	31652.4	15140.0	100/100
	25	0.423	0.420	0.480	53598.0	25297.7	100/100
<i>Ditch</i>	1	0.640	0.640	0.640	6218.1	2294.4	34/100
	5	0.640	0.640	0.640	17250.0	6750.3	100/100
	10	0.640	0.640	0.640	25333.2	10171.4	100/100
	25	0.640	0.640	0.640	42419.5	17402.7	100/100
<i>Corridor</i>	1	0.400	0.400	0.400	6437.1	2035.2	26/100
	5	0.400	0.400	0.400	20834.9	5288.8	92/100
	10	0.400	0.400	0.400	33405.4	8035.9	99/100
	25	0.400	0.400	0.400	61279.5	13747.2	100/100
<i>Maze</i>	1	0.480	0.480	0.480	6170.1	2455.4	24/100
	5	0.480	0.480	0.480	20751.2	8991.1	99/100
	10	0.480	0.480	0.480	33049.3	14808.7	100/100
	25	0.480	0.480	0.480	57441.5	26592.6	100/100
<i>Spacious</i>	1	0.346	0.000	0.400	5961.4	3254.5	97/100
	5	0.248	0.000	0.400	20470.8	11047.0	100/100
	10	0.212	0.000	0.400	32485.0	17641.2	100/100
	25	0.168	0.000	0.400	57866.5	30630.2	100/100

Table 3.2. Performance of the off-line footstep planner when minimizing the height variation.

Scenario	Time Budget [s]	Avg Cost	Min Cost	Max Cost	Iters	Tree Size	Successes
<i>Rod</i>	1	30.060	20.556	58.287	4925.5	2143.6	92/100
	5	25.480	18.266	42.102	16219.7	6785.2	100/100
	10	23.142	17.586	36.173	26342.3	10602.8	100/100
	25	20.331	17.627	27.902	48444.6	18275.1	100/100
<i>Ditch</i>	1	78.095	58.308	98.540	4200.6	1446.2	10/100
	5	72.377	54.725	99.004	13681.3	4456.7	96/100
	10	64.840	49.282	83.708	21817.8	7302.6	100/100
	25	55.466	44.438	71.903	39632.2	13139.3	100/100
<i>Corridor</i>	1	94.234	72.764	112.454	4538.3	1376.9	12/100
	5	97.323	73.304	139.995	15477.9	3418.1	82/100
	10	88.866	66.266	139.700	26354.5	5314.1	98/100
	25	78.178	64.615	102.587	52076.3	9236.0	100/100
<i>Maze</i>	1	107.971	95.340	127.139	4374.8	1744.1	8/100
	5	106.620	81.630	149.408	16037.0	5919.7	88/100
	10	99.264	73.844	133.529	27154.9	10394.0	100/100
	25	84.433	65.234	119.569	52035.2	19752.6	100/100
<i>Spacious</i>	1	52.476	32.652	85.874	4467.9	2286.9	97/100
	5	47.138	30.160	70.100	15879.2	7689.2	100/100
	10	43.535	28.001	66.777	26325.6	12425.1	100/100
	25	38.048	27.357	57.544	49981.9	22038.9	100/100

Table 3.3. Performance of the off-line footstep planner when maximizing the minimum clearance.

through a graph-SLAM algorithm and a loop closure detector. It is worth mentioning that our architecture is independent from the specific implementation of the localization module, hence any off-the-shelf visual SLAM method can be employed in place of RTAB-Map (see assumption A3 in Sect. 3.2).

Given the pose \hat{s} of the camera frame estimated through visual SLAM and the measured joint positions, the direct kinematics module produces the estimates \hat{p}_c and $\hat{\varphi}$ of, respectively, the CoM position and swing foot pose. These are then provided to the gait generation and kinematic control module to achieve closed-loop control.

3.3.4 Simulations

We performed simulations on the HRP-4 humanoid robot in the CoppeliaSim environment. We tested our off-line framework in multiple environments (Fig. 3.7). For the gait generation module we have set $\eta = 3.6 \text{ s}^{-1}$, the single support duration $T_{ss} = 0.6 \text{ s}$, the double support duration $T_{ds} = 0.4 \text{ s}$, the size of the moving box $\tilde{d}_x^z = \tilde{d}_y^z = d_z^z = 0.05 \text{ m}$, $\beta = 1000$, $C = 100$ and $\delta = 0.01 \text{ s}$. To solve the QP problems we used `hpiqm`, which requires less than 1 ms to solve each QP and is thus able to run in real-time with an ample margin.

Figure 3.10 shows the robot traversing the scenario *Ditch*. The robot starts by moving to its left (first snapshot), approaching the accessible patch (second snapshot). It then accesses the platform in the middle correctly avoiding the obstacle (third and fourth snapshots), eventually reaching the goal region by climbing the final two patches (fifth and sixth snapshots). Figure 3.11 shows the robot moving inside the scenario *Corridor*. The robot first exits the room in which it starts (first and second snapshots), approaching the stairway (third snapshot). Then, it goes up and down the staircases avoiding the obstacles (fourth and fifth snapshots), finally reaching the goal region (sixth snapshot).

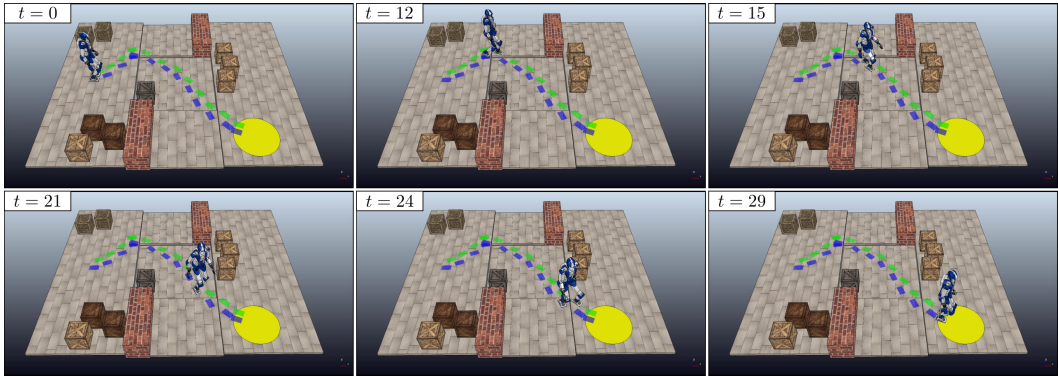


Figure 3.10. The robot reaches the goal going through the ditch, which can only be accessed from the left and exited from the right.

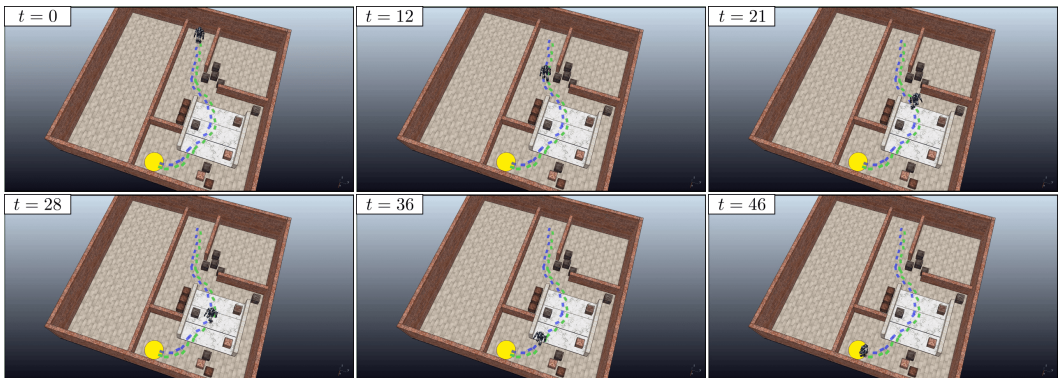


Figure 3.11. The robot reaches the goal avoiding the corridor, climbing and descending the staircase while avoiding the obstacles.

In order to verify the validity of Assumption A4, we computed the ground reaction forces associated with the generated trajectories, and verified that the no-slipping condition is always satisfied. Indeed, in our simulations the ratio between the horizontal and vertical components of the ground reaction force peaks around 0.1, which is a completely acceptable value under normal circumstances (e.g., steel-concrete friction coefficients are normally not lower than 0.5 [26]).

We invite the reader to watch the accompanying video, which includes clips related to the above simulations as well as additional cases.

3.4 The on-line case

We now extend the proposed method to the on-line case. This section starts with a description of the general architecture which, compared to that proposed for the off-line case, includes two additional modules, i.e., the mapping and visual task generation module, and employs a sensor-based version of the footstep planner, which will now work on-line; all the other modules, in particular gait generation, remain instead identical. Then, we describe the mentioned components and present some simulation results.

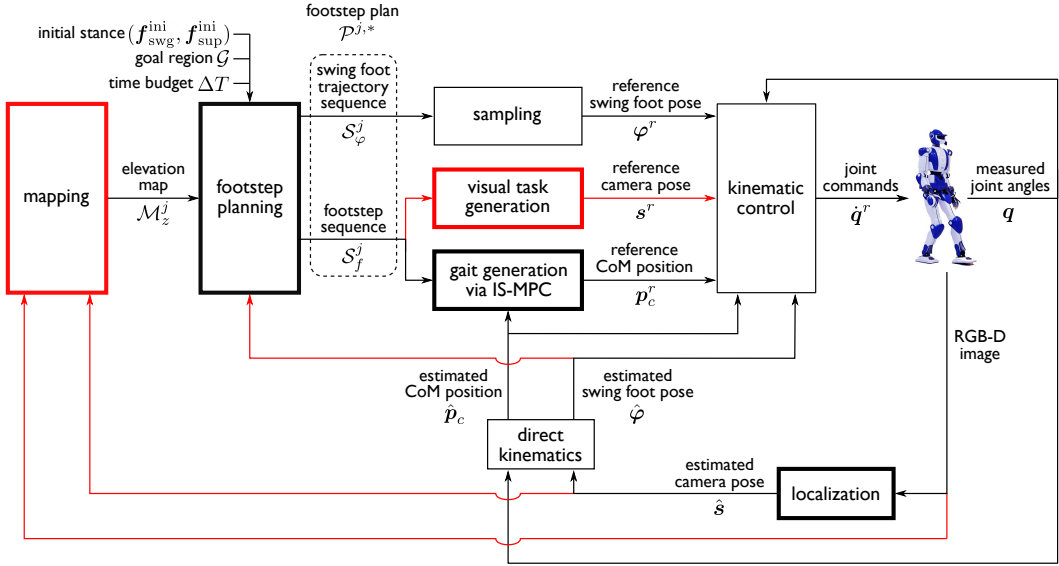


Figure 3.12. Block scheme of the on-line case. The red blocks and arrows highlight the additional modules and signals compared to the off-line case.

3.4.1 General architecture

The proposed architecture for the on-line case is given in Fig. 3.12, where the additional modules and feedback signals are shown in red.

At the beginning, the map \mathcal{M}_z is initialized combining some limited exogenous knowledge about the starting location of the robot and information available by the head-mounted camera at its initial pose. Such initial map \mathcal{M}_z^0 , together with the initial humanoid stance ($\mathbf{f}_{\text{swg}}^{\text{ini}}, \mathbf{f}_{\text{sup}}^{\text{ini}}$), the goal region \mathcal{G} and a preassigned time budget ΔT , is provided to the footstep planner to find a first (possibly partial) footstep plan $\mathcal{P}^{1,*} = \{\mathcal{S}_f^1, \mathcal{S}_{\varphi}^1\}$.

After this initial off-line phase, all the modules run in parallel, generating the humanoid motions in a sensor-based, closed-loop fashion. The mapping module incrementally builds the elevation map \mathcal{M}_z using the RGB-D images acquired by the humanoid while walking and the estimate \hat{s} of the camera pose produced by the localization module. To account for changes in \mathcal{M}_z and take advantage of newly acquired information, the footstep plan is on-line updated and/or extended by repeatedly invoking the footstep planner at every step of the humanoid, with the ultimate objective of reaching \mathcal{G} .

More precisely, consider the generic timestamp t_s^j , i.e., the beginning of the j -th step. Let $(\hat{\mathbf{f}}_{\text{swg}}^j, \hat{\mathbf{f}}_{\text{sup}}^j)$ be the current stance, with $\hat{\mathbf{f}}_{\text{swg}}^j$ and $\hat{\mathbf{f}}_{\text{sup}}^j$ the estimates of the swing and support foot poses at t_s^j , and $\mathcal{P}^{j,*} = \{\mathcal{S}_f^j, \mathcal{S}_{\varphi}^j\}$ be the current footstep plan – computed during the previous $((j-1)\text{-th})$ step – where the sequences of footstep placements and associated swing trajectories are defined as

$$\begin{aligned}\mathcal{S}_f^j &= \{\mathbf{f}^{j|j}, \dots, \mathbf{f}^{j+n|j}\}, \\ \mathcal{S}_{\varphi}^j &= \{\varphi^{j|j}, \dots, \varphi^{j+n-2|j}\}\end{aligned}$$

with their generic elements $\mathbf{f}^{j+i|j}$ and $\varphi^{j+i|j}$ denoting, respectively, the $(j+i)$ -

th footstep and trajectory produced by the j -th planner invocation, $\mathbf{f}^{j|j} \approx \hat{\mathbf{f}}_{\text{swg}}^j$, $\mathbf{f}^{j+1|j} \approx \hat{\mathbf{f}}_{\text{sup}}^j$ and the last footstep $\mathbf{f}^{j+n|j}$ henceforth referred to as *subgoal*. Also, let $(\mathbf{f}_{\text{swg}}^{j+1}, \mathbf{f}_{\text{sup}}^{j+1})$ be the stance that the humanoid is supposed to achieve at $t_s^{j+1} = t_s^j + T_s^j$, with $\mathbf{f}_{\text{swg}}^{j+1} = \hat{\mathbf{f}}_{\text{sup}}^j$ and $\mathbf{f}_{\text{sup}}^{j+1} = \mathbf{f}^{j+2|j}$, after performing the swing trajectory $\varphi^{j|j}$ having duration T_s^j . Then, during the time interval $[t_s^j, t_s^{j+1}]$, motion execution and footstep planning take place simultaneously as follows.

- At any time instant $t \in [t_s^j, t_s^{j+1}]$, the current reference position \mathbf{p}_c^r of the CoM is produced by the gait generator, based on the sequence \mathcal{S}_f^j , similarly to the off-line case; the current reference pose φ^r of the swing foot is obtained by sampling the trajectory $\varphi^{j|j}$; moreover, the visual task generator produces the reference pose \mathbf{s}^r of the camera frame, given its current estimate $\hat{\mathbf{s}}$ and the sequence \mathcal{S}_f^j , that allows to direct the gaze towards the subgoal extracted from \mathcal{S}_f^j , and then to enlarge \mathcal{M}_z in the area of the current destination. References \mathbf{p}_c^r , φ^r , \mathbf{s}^r , together with their estimates $\hat{\mathbf{p}}_c$, $\hat{\varphi}$, $\hat{\mathbf{s}}$, are passed to the kinematic controller to compute the joint commands $\dot{\mathbf{q}}^r$ for the robot.
- At t_s^j , the footstep planner is invoked providing in input the stance $(\mathbf{f}_{\text{swg}}^{j+1}, \mathbf{f}_{\text{sup}}^{j+1})$, the goal region \mathcal{G} , a time budget equal to T_s^j , and the elevation map \mathcal{M}_z^j currently available by the mapping module. At t_s^{j+1} , the planner returns a new footstep plan $\mathcal{P}^{j+1,*} = \{\mathcal{S}_f^{j+1}, \mathcal{S}_\varphi^{j+1}\}$, where the sequences \mathcal{S}_f^{j+1} and $\mathcal{S}_\varphi^{j+1}$ are defined similarly to \mathcal{S}_f^j and \mathcal{S}_φ^j , $\mathbf{f}^{j+1|j+1} = \mathbf{f}_{\text{swg}}^{j+1}$ and $\mathbf{f}^{j+2|j+1} = \mathbf{f}_{\text{sup}}^{j+1}$. The first element $\varphi^{j+1|j+1}$ of $\mathcal{S}_\varphi^{j+1}$ will define the next $((j+1)$ -th) step of the humanoid.

Note that, while the footstep planner will make use of a fixed map \mathcal{M}_z^j during the time interval $[t_s^j, t_s^{j+1}]$, the map \mathcal{M}_z will continuously be updated by the mapping module during the same time interval, which will generally provide a different map \mathcal{M}_z^{j+1} for the next invocation of the planner.

Clearly, in the on-line case, only the quality of the partial footstep plans can be accounted for, ultimately leading to an overall plan that is globally suboptimal.

3.4.2 Mapping

At the generic time instant, the mapping module receives in input the last RGB-D image acquired by the head-mounted camera and the current estimate $\hat{\mathbf{s}}$ of the camera pose produced by the localization module. It is responsible for integrating such newly acquired information into the elevation map \mathcal{M}_z .

First, the depth data extracted from the RGB-D image are used to construct a point cloud. Then, the latter is given in input, together with the estimate $\hat{\mathbf{s}}$ and a sensor noise model, to Elevation Mapping [27], an open source framework designed for rough terrain mapping; this accordingly updates a local (limited around the robot) representation of the environment in the form of a 2.5D grid map (see Assumption A1). Finally, such local map is integrated into \mathcal{M}_z in order to maintain a global representation of the explored area of the environment.

The mapping module, at the time t_s^j of the generic j -th invocation of the footstep planner, provides it with a copy \mathcal{M}_z^j of the available map \mathcal{M}_z . Meanwhile, during

the planner operation, the map \mathcal{M}_z is continuously updated through the process described above.

3.4.3 Sensor-based footstep planning

This module consists in a sensor-based version of the footstep planner proposed in Sect. 3.3.2 which works using the knowledge about the environment incrementally acquired by the robot during motion.

The input data for the j -th invocation of the footstep planner are the next robot stance $(\mathbf{f}_{\text{swg}}^{j+1}, \mathbf{f}_{\text{sup}}^{j+1})$, the goal region \mathcal{G} , the time budget ΔT^j and the elevation map \mathcal{M}_z^j . Given an optimality criterion, the footstep planner returns the best footstep plan $\mathcal{P}^{j+1,*}$, found within ΔT^j , either leading to \mathcal{G} or terminating in proximity of the frontier of \mathcal{M}_z^j . The latter case is typical whenever \mathcal{G} is not included in \mathcal{M}_z^j , e.g., due to occlusions or simply being placed far from the robot.

The planning algorithm builds a tree \mathcal{T}^{j+1} reusing portions of the tree \mathcal{T}^j built up to the previous invocation. In this tree, vertexes and edges are defined as described in Sect. 3.3.2, with the only difference that a vertex $v = (\mathbf{f}_{\text{swg}}, \mathbf{f}_{\text{sup}})$ can contain a support footstep \mathbf{f}_{sup} whose z -coordinate is unspecified, indicating that \mathcal{M}_z^j does not provide enough information (in a sense formally defined in the following) about the ground under the foot at \mathbf{f}_{sup} . Vertexes with this characteristic represent stances located on the frontier of \mathcal{M}_z^j and thus indicate possible direction for further exploration of the environment. The generic invocation consists of: initializing, updating and expanding the tree. These individual steps are described in the following.

Initializing: The vertex $v^{\text{root}} = (\mathbf{f}_{\text{swg}}^{\text{root}}, \mathbf{f}_{\text{sup}}^{\text{root}})$ of \mathcal{T}^j that is closest to $(\mathbf{f}_{\text{swg}}^{j+1}, \mathbf{f}_{\text{sup}}^{j+1})$ is identified. To this end, we define a stance-to-stance metric as

$$\zeta(v, v') = \gamma(\mathbf{f}_{\text{swg}}, \mathbf{f}'_{\text{swg}}) + \gamma(\mathbf{f}_{\text{sup}}, \mathbf{f}'_{\text{sup}}) \quad (3.9)$$

where $\gamma(\cdot)$ is the footstep-to-footstep metric defined in (3.4). The subtree of \mathcal{T}^j rooted at v^{root} is extracted (including v^{root} itself) and represents the initial version of \mathcal{T}^{j+1} . To match the stance that the humanoid is supposed to reach at the end of the simultaneously executed step, v^{root} is modified by relocating $\mathbf{f}_{\text{swg}}^{\text{root}}$ to $\mathbf{f}_{\text{swg}}^{j+1}$ and $\mathbf{f}_{\text{sup}}^{\text{root}}$ to $\mathbf{f}_{\text{sup}}^{j+1}$. \blacktriangleleft

Updating: At this point, requirements R1–R3 are satisfied by construction in \mathcal{T}^{j+1} according to the previous map \mathcal{M}_z^{j-1} . Then, R1–R3 must now be checked in \mathcal{T}^{j+1} using the most recent map \mathcal{M}_z^j , consequently updating vertexes and edges in order to satisfy them. To this end, we perform a pre-order traversal of \mathcal{T}^{j+1} as described in the following.

When a vertex $v = (\mathbf{f}_{\text{swg}}, \mathbf{f}_{\text{sup}})$ is visited, it is modified⁹ by relocating its swing footstep to the support footstep $\mathbf{f}_{\text{sup}}^{\text{parent}}$ of its parent $v^{\text{parent}} = (\mathbf{f}_{\text{swg}}^{\text{parent}}, \mathbf{f}_{\text{sup}}^{\text{parent}})$, and setting the z coordinate $z_{f,\text{sup}}$ of \mathbf{f}_{sup} according to \mathcal{M}_z^j . In particular, consider the cells of \mathcal{M}_z^j belonging to, or overlapping with, the footprint at \mathbf{f}_{sup} ; let n_k and n_u be the number of these cells whose height is known and unknown, respectively. If

⁹This modification is not made on v^{root} as it corresponds to the stance that the robot must reach at the end of the simultaneously executed step.

the rate of cells with known height is larger than a predefined threshold \bar{n} , i.e.,

$$\frac{n_k}{n_k + n_u} > \bar{n},$$

$z_{f,\text{sup}}$ is set to the average value of the n_k known heights. Otherwise, $z_{f,\text{sup}}$ is left unspecified.

Once v has been updated, requirements R1–R3 are checked similarly to what was done in the off-line case, with the only two differences described in the following.

- If $z_{f,\text{sup}}$ is unspecified, requirements R1–R3 are checked conjecturing that it is equal to the z -component $z_{f,\text{swg}}$ of \mathbf{f}_{swg} .
- Requirement R1 is considered satisfied if for each of the n_k known heights, the net variation from $z_{f,\text{sup}}$ does not exceed a predefined threshold \bar{z} , i.e.,

$$|z_k - z_{f,\text{sup}}| \leq \bar{z}.$$

with z_k the generic known height among the n_k available.

If any requirement among R1–R3 is violated, vertex v is removed from \mathcal{T}^{j+1} , along with its descendants. Otherwise, the edge connecting v to v^{parent} is replaced by the trajectory φ^{parent} generated while checking R3; the set $\mathcal{V}_{\text{child}}$ of child vertexes of v is retrieved, and the procedure is recursively invoked on them. To guarantee on-line performance and save time to be used for expanding \mathcal{T}^{j+1} , recursion is stopped on vertexes having a maximum depth $\bar{\kappa}$. \blacktriangleleft

Expanding: Once \mathcal{T}^{j+1} has been updated, it can be further expanded in the map \mathcal{M}_z^j . Let ΔT_e be the time elapsed since the beginning of the current invocation of the footstep planner, i.e., the time spent in initializing and updating \mathcal{T}^{j+1} . The expansion of \mathcal{T}^{j+1} works iteratively as described in Sect. 3.3.2 using the remaining portion of the time budget $\Delta T^j - \Delta T_e$ and the map \mathcal{M}_z^j , with the following modifications.

- The choice of the z -coordinate for a candidate footstep $\mathbf{f}_{\text{sup}}^{\text{cand}}$ and the check of requirements R1–R3 are done exactly as when updating a generic vertex.
- A vertex whose support footstep has unspecified z -coordinate cannot be set as parent of another vertex. Then, such vertexes are excluded both when selecting the vertex v^{near} for an expansion attempt and when choosing a parent for a candidate vertex v^{cand} . \blacktriangleleft

Similarly to the off-line case, when the assigned time budget ΔT^j runs out, tree expansion is stopped and the set $\mathcal{V}_{\text{goal}}$ of vertexes v such that $\mathbf{p}_{f,\text{sup}} \in \mathcal{G}$ is retrieved. If $\mathcal{V}_{\text{goal}}$ is not empty, the vertex v^* with minimum cost is selected as in (3.8). Otherwise, if $\mathcal{V}_{\text{goal}}$ is empty, the planner retrieves the set $\mathcal{V}_{\text{fron}}$ containing all vertexes of \mathcal{T}^{j+1} having at least one child vertex whose support footstep has unspecified z -coordinate. In practice, vertexes in $\mathcal{V}_{\text{fron}}$ contain stances located in proximity of the frontier of the current map \mathcal{M}_z^j . Then, the vertex v^* is selected as

$$v^* = \operatorname{argmin}_{v \in \mathcal{V}_{\text{fron}}} c(v) + g(v) \quad (3.10)$$

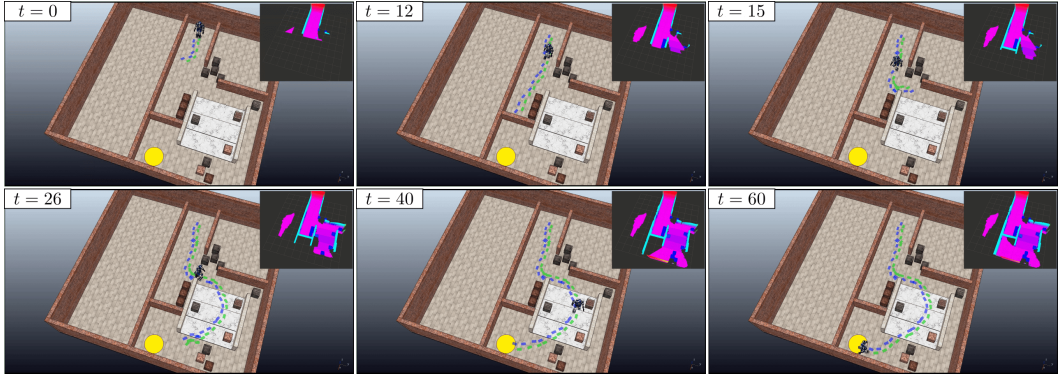


Figure 3.13. The on-line footstep planner in the scenario *Corridor* minimizing the number of steps. Here the planner finds a footstep sequence of 54 steps.

where $g(v)$ represents the *cost-to-go* of vertex v , i.e., a lower-bound on the minimum cost to reach \mathcal{G} from v . A possible choice for $g(v)$ when minimizing the number of steps along the plan will be described in Sect. 3.4.5.

Finally, the footstep plan $\mathcal{P}^{j+1,*}$ is retrieved from the branch of \mathcal{T}^{j+1} joining the root to v^* . Clearly, if $\mathcal{V}_{\text{goal}}$ is not empty, $\mathcal{P}^{j+1,*}$ will be a complete footstep plan leading to \mathcal{G} ; otherwise, $\mathcal{P}^{j+1,*}$ will be a partial footstep plan leading in the direction of an unknown area of the environment whose exploration is considered useful – according to the adopted cost-to-go – to proceed towards \mathcal{G} .

3.4.4 Visual task generation

At any time instant during the execution of the generic j -th step, given the current estimate \hat{s} of the camera pose and the subgoal $f^{j+n|j}$, which is readily extracted from the current sequence \mathcal{S}_f^j of footstep placements, the visual task generator is in charge of producing a suitable reference s^r of the camera pose which aims at directing the gaze towards the current destination of the robot. The rationale beyond this choice is that, since the current footstep plan terminates in an area on the frontier of the map \mathcal{M}_z that is considered promising for goal-oriented exploration of the environment, looking in the direction of $f^{j+n|j}$ allows to enlarge the map in that particular area. In principle, whenever possible, this will privilege further extension of the footstep plan in that promising direction.

To compute s^r , one possibility consists in adopting an image-based visual servoing scheme [28]. In particular, one may define a virtual feature in the image plane of the camera at \hat{s} associated to the representative point $p_f^{j+n|j}$ of the subgoal footstep $f^{j+n|j}$. Then, the reference pose s^r of the camera frame can be computed so as to keep such feature at the center of the image plane.

The produced reference pose s^r is passed to the kinematic controller which, in practice, only controls the camera yaw and pitch angles.

3.4.5 Simulations

In this section we present simulations obtained with the discussed architecture for the on-line case. Parameters are set to the same values of Sects. 3.3.2 and 3.3.4, with

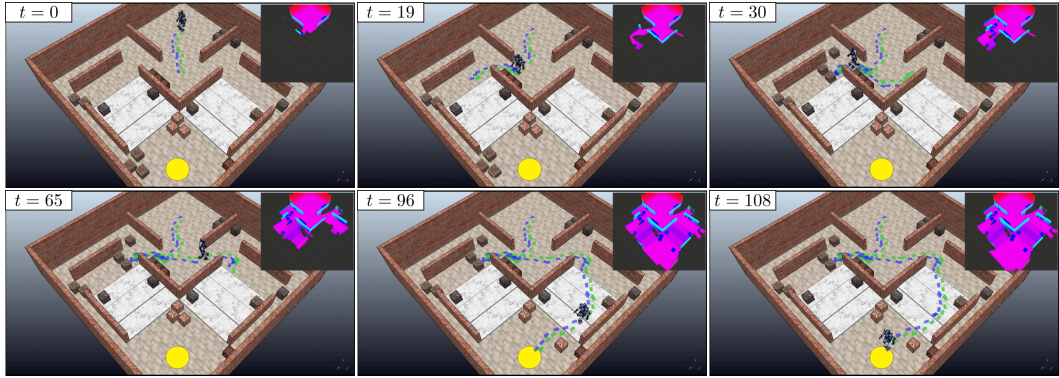


Figure 3.14. The on-line footstep planner in the environment *Maze* minimizing the number of steps. The environment is dynamic, namely the elevation map can be changed by moving obstacles around. Here the planner finds a footstep sequence of 106 steps.

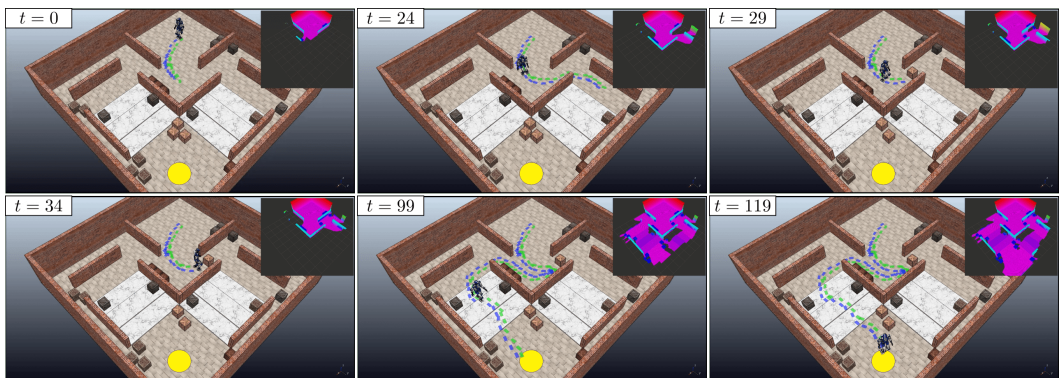


Figure 3.15. The on-line footstep planner in the dynamic environment *Maze* minimizing the number of steps. Here the planner finds a footstep sequence of 103 steps.

the only exception of setting $k_\gamma = 1$ in (3.4) when used in (3.9), $\bar{n} = 0.9$, $\bar{z} = 0.02$ and $\bar{\kappa} = 5$. For each j -th invocation of the footstep planner the time budget ΔT^j is set to $T_{ss} + T_{ds}$. In all performed simulations, the quality criteria considered by the footstep planner is the number of steps, while the *cost-to-go* of each vertex v is an underestimation of the number of steps needed to reach the goal region \mathcal{G} from the double support configuration specified by v . This value is computed as the distance between the position of the support foot specified by v and \mathcal{G} , divided by the longest step among the catalogue of primitives U .

Figure 3.13 shows the robot walking in the scenario *Corridor* together with the reconstructed elevation map. Here, the planner continuously receives an updated version of the map, which is built while the robot moves. Initially (first snapshot) the robot starts exploring its surrounding environment, moving towards the end of the corridor (second snapshot). As soon as the footstep planner realizes that the room is closed, it replans a sequence of footsteps which brings the robot outside the corridor (third snapshot). The robot keeps exploring the environment, going up and down the stairs and avoiding the obstacles placed along the path (fourth and fifth snapshot). Finally, the robot reaches the desired goal region (sixth snapshot).

Figure 3.14 shows the robot accomplishing the locomotion task in the scenario *Maze*. In this case the scenario was rendered dynamic by manually moving the obstacles at runtime. Here, the planner is facing the additional challenge of operating under continuous changes in the elevation map, which reflects the new locations of the obstacles. The robot starts by moving outside the initial room (first snapshot), choosing the path on its right (second snapshot). The footstep plan is invalidated by placing obstacles in front of the robot, forcing the robot to choose the other direction (third snapshot). The footstep planner correctly drives the robot towards the other area of the maze (fourth snapshot), making it go up and down the staircase (fifth snapshot), avoiding another obstacle which is placed in front of the robot right before reaching the goal region (sixth snapshot).

Figure 3.15 shows a situation, again in a dynamic version of the scenario *Maze*, in which the planner reaches a point in which is not able to find a new subgoal. This occurs when, once the time budget expires, both $\mathcal{V}_{\text{goal}}$ and $\mathcal{V}_{\text{fron}}$ are empty. For example, this may happen when the humanoid must exit a long corridor or when dynamic obstacles invalidate large portion of the created tree. In this specific situation, a simple solution consists in keeping the portion of the current footstep plan that is still valid after the updating step of the planner. If this happens multiple times in a row, the robot reaches the subgoal and stops. At this point, the footstep planner is invoked with an unlimited time budget and terminates as soon as a new subgoal is found. As before, the robot starts by moving outside the initial room, moving towards its left (first and second snapshots). The footstep plan is invalidated by moving an obstacle in front of the robot (third snapshots), which stops its motion upon reaching the current subgoal (fourth snapshot). As soon as the footstep planner finds a new subgoal, the robot starts moving again (fifth snapshot), eventually reaching the desired goal region (sixth snapshot).

Clips of the described simulations are included in the accompanying video.

3.5 Discussion

The proposed approach integrates several components and is designed to work both off-line and on-line. Since, to the best of our knowledge, no existing method can address the same wide range of situations, we focus in the following on the two main components (footstep planning and gait generation) separately.

As a representative of the state of the art in footstep planning, we selected the algorithm in [11], which uses a weighted A^* algorithm to search for optimal footstep sequences on uneven ground¹⁰. At each iteration, the vertex providing the lowest estimate for the path cost is expanded. This estimate is computed by adding to the cost of the vertex a heuristic cost-to-go, given by the distance to the goal divided by the maximum step length and multiplied by a weight $w \geq 1$, which can be used to increase the bias towards the goal region. The main difference with respect to our approach lies in the expansion mechanism, which is deterministic in [11] and probabilistic in our method.

Both our scheme and the weighted A^* approach use a catalogue of primitives. In order to perform a fair comparison, we use for the weighted A^* approach the same catalogue described in Sect. 3.3.2. As for the optimality criterion, we aim to minimize the number of footsteps, corresponding to an edge cost given by (3.5). In order to allow for the possibility that our implementation might not be the most efficient, we assigned to the weighted A^* planner a time budget of 100 s, which is four times the largest budget used when testing our planner.

The results obtained showed that standard A^* search, corresponding to $w = 1$, is unable to find solutions within the allotted time budget in any of the considered scenarios. By increasing w , weighted A^* performs rather well in scenarios where the solution does not involve considerable backtracking (*Rod* and *Spacious*), but fails to find the solution in any other scenario. In particular, Table 3.4 collects the results obtained for $w = 5$. These results should be compared to those in Table 3.1, which show that our approach has a 100% success rate with a fourth of the time budget. We also ran tests with larger weights ($w = 10$, $w = 25$), obtaining results that are essentially identical, with slightly longer paths and no increase in the success rate.

Indeed, the outcome of the above comparison was rather predictable. It is well known that weighted A^* works quite well in environments where the path leading to the goal does not deviate significantly from a straight line. However, as acknowledged by the authors of [11], its performance may degrade severely in the scenarios that require even mild amounts of backtracking.

As for the gait generation component, there are several alternatives to our method that employ MPC on reduced-order models. The advantage of the proposed approach lies in the introduction of the stability constraint, which allows to prove rigorously recursive feasibility and internal stability of the MPC scheme. The effectiveness of this approach was extensively analyzed in [20], by means of comparisons to state-of-the-art schemes. What we proposed in this paper is an extension accounting for the fact that the CoM height changes. Based on the additional theoretical results which we proved (namely, Props. 2 and 3), we can claim that our 3D gait generation

¹⁰The algorithm in [11] actually contemplates the possibility of tilted surfaces, but obviously works in a world of stairs as a particular case.

Scenario	Cost	Iters	Tree Size
<i>Rod</i>	22.0	650	4049
<i>Ditch</i>	Fail	11687	21911
<i>Corridor</i>	Fail	12343	22483
<i>Spacious</i>	31.0	34	546
<i>Maze</i>	Fail	9546	22333

Table 3.4. Performance of the off-line weighted A^* footstep planner when minimizing the number of steps ($w = 5.0$).

retains the same properties of the original 2D scheme.

3.6 Conclusions

In this paper, we addressed the problem of motion generation for a humanoid robot that must reach a certain goal region walking in an environment consisting of horizontal patches located at different heights, called *world of stairs*. We considered two versions of such problem: the off-line and on-line case. In the first, the geometry of the environment is completely known in advance, while in the second, it is reconstructed by the robot itself during motion using an on-board sensor. In both cases, available information about the environment is maintained in the form of an elevation map.

For the off-line case, we proposed an architecture working in two main stages: footstep planning and gait generation. First, a feasible footstep plan leading to the goal region is off-line computed using a randomized algorithm that takes into account the plan quality specified by a given optimality criterion. Then, an intrinsically stable MPC-based scheme computes a CoM trajectory that realizes the found footstep sequence, while guaranteeing dynamic balance and boundedness of the CoM w.r.t. the ZMP at all time instants.

For the on-line case, we proposed an extension of the architecture for the off-line case where footstep plans are computed in parallel to gait generation and map building. To this end, we presented a sensor-based version of the footstep planner that uses the knowledge about the environment incrementally acquired by the robot during motion.

We validated the proposed architectures by providing simulation results obtained in CoppeliaSim on the HRP-4 humanoid robot in scenarios of different complexity.

Our future work will explore several directions, such as

1. providing a formal proof of asymptotic optimality of the proposed footstep planner;
2. developing a more general version of the proposed approach to deal with arbitrary terrains, removing the world of stairs assumption;
3. implementing the presented architectures on a real humanoid robot;
4. extending them to the case of large-scale and multi-floor environments.

3.6.1 Pseudocode

We report here a pseudocode description of the footstep planners presented in Sections 3.3.2 and 3.4.3, along with the relevant procedures.

Algorithm 1: FootstepPlanner

Input: $(\mathbf{f}_{\text{swg}}^{\text{ini}}, \mathbf{f}_{\text{sup}}^{\text{ini}}), \mathcal{G}, \Delta T, \mathcal{M}_z$

Output: \mathcal{P}^*

- 1 $v^{\text{ini}} \leftarrow (\mathbf{f}_{\text{swg}}^{\text{ini}}, \mathbf{f}_{\text{sup}}^{\text{ini}});$
 - 2 AddVertex($\mathcal{T}, \emptyset, v^{\text{ini}}, \emptyset$);
 - 3 ExpandTree($\mathcal{T}, \Delta T, \mathcal{M}_z$);
 - 4 $\mathcal{P}^* \leftarrow \text{RetrieveBestPlan}(\mathcal{T}, \mathcal{G});$
 - 5 **return** \mathcal{P}^* ;
-

Procedure 1: ExpandTree

Input: $\mathcal{T}, \Delta T, \mathcal{M}_z$

Output: none

- 1 **while** not TimeExpired(ΔT) **do**
 - 2 $\mathbf{p}_{xy}^{\text{rand}} \leftarrow \text{SamplePoint}();$
 - 3 $v^{\text{near}} \leftarrow \text{NearestVertex}(\mathcal{T}, \mathbf{p}_{xy}^{\text{rand}});$
 - 4 $\mathbf{f}_{\text{sup}}^{\text{cand}} \leftarrow \text{GenerateCandidateFootstep}(\mathbf{f}_{\text{sup}}^{\text{near}}, U, \mathcal{M}_z);$
 - 5 **if** R1($\mathbf{f}_{\text{sup}}^{\text{cand}}$) **and** R2($\mathbf{f}_{\text{sup}}^{\text{cand}}, \mathbf{f}_{\text{sup}}^{\text{near}}$) **then**
 - 6 $\varphi^{\text{near}} \leftarrow \text{SwingTrajectoryEngine}(\mathbf{f}_{\text{swg}}^{\text{near}}, \mathbf{f}_{\text{sup}}^{\text{cand}});$
 - 7 **if** R3($\varphi^{\text{near}}, (\mathbf{f}_{\text{sup}}^{\text{near}}, \mathbf{f}_{\text{sup}}^{\text{cand}})$) **then**
 - 8 $v^{\text{cand}} \leftarrow (\mathbf{f}_{\text{sup}}^{\text{near}}, \mathbf{f}_{\text{sup}}^{\text{cand}});$
 - 9 $\mathcal{N} \leftarrow \text{Neighbors}(\mathcal{T}, v^{\text{cand}});$
 - 10 $(v^{\text{min}}, \varphi^{\text{min}}) \leftarrow \text{ChooseParent}(\mathcal{T}, \mathcal{N}, v^{\text{near}}, v^{\text{cand}}, \varphi^{\text{near}});$
 - 11 $v^{\text{new}} \leftarrow (\mathbf{f}_{\text{sup}}^{\text{min}}, \mathbf{f}_{\text{sup}}^{\text{cand}});$
 - 12 AddVertex($\mathcal{T}, v^{\text{min}}, v^{\text{new}}, \varphi^{\text{min}}$);
 - 13 ReWire($\mathcal{T}, \mathcal{N}, v^{\text{new}}$);
 - 14 **end**
 - 15 **end**
 - 16 **end**
 - 17 **return**;
-

Procedure 2: SwingTrajectoryEngine

Input: f^a, f^b
Output: φ^a

```

1  $h \leftarrow h^{\min};$ 
2 while  $h \leq h^{\max}$  do
3    $\varphi^a \leftarrow \text{DeformTrajectory}(f^a, f^b, h);$ 
4   if CollisionFree( $\varphi^a$ ) then
5     return  $\varphi^a;$ 
6   end
7    $h \leftarrow h + \Delta h;$ 
8 end
9 return  $\emptyset;$ 

```

Procedure 3: ChooseParent

Input: $\mathcal{T}, \mathcal{N}, v^{\text{near}}, v^{\text{cand}}, \varphi^{\text{cand}}$
Output: v^{\min}, φ^{\min}

```

1  $v^{\min} \leftarrow v^{\text{near}};$ 
2  $\varphi^{\min} \leftarrow \varphi^{\text{cand}};$ 
3  $c^{\min} \leftarrow c(v^{\text{near}}) + l(v^{\text{near}}, v^{\text{cand}});$ 
4 foreach  $v' \in \mathcal{N}$  do
5   if R2( $f_{\text{sup}}^{\text{cand}}, f'_{\text{sup}}$ ) then
6      $\varphi' \leftarrow \text{SwingTrajectoryEngine}(f'_{\text{swg}}, f_{\text{sup}}^{\text{cand}});$ 
7     if R3( $\varphi', (f'_{\text{sup}}, f_{\text{sup}}^{\text{cand}})$ ) and  $c(v') + l(v', v^{\text{cand}}) < c^{\min}$  then
8        $v^{\min} \leftarrow v';$ 
9        $\varphi^{\min} \leftarrow \varphi';$ 
10       $c^{\min} \leftarrow c(v') + l(v', v^{\text{cand}});$ 
11    end
12  end
13 end
14 return  $(v^{\min}, \varphi^{\min});$ 

```

Procedure 4: ReWire

Input: $\mathcal{T}, \mathcal{N}, v^{\text{new}}$
Output: none

```

1 foreach  $v' \in \mathcal{N}$  do
2   if  $R2(\mathbf{f}'_{\text{sup}}, \mathbf{f}^{\text{new}}_{\text{sup}})$  then
3      $\varphi^{\text{new}} \leftarrow \text{SwingTrajectoryEngine}(\mathbf{f}^{\text{new}}_{\text{swg}}, \mathbf{f}'_{\text{sup}});$ 
4     if  $R3(\varphi^{\text{new}}, (\mathbf{f}'_{\text{swg}}, \mathbf{f}'_{\text{sup}}))$  and  $c(v^{\text{new}}) + l(v^{\text{new}}, v') < c(v')$  then
5       UpdateVertex( $\mathcal{T}, v', (\mathbf{f}^{\text{new}}_{\text{sup}}, \mathbf{f}'_{\text{sup}})$ );
6       UpdateEdge( $\mathcal{T}, v^{\text{new}}, v', \varphi^{\text{new}}$ );
7        $\mathcal{V}_{\text{child}} \leftarrow \text{ChildVertexes}(\mathcal{T}, v');$ 
8       foreach  $v'' \in \mathcal{V}_{\text{child}}$  do
9          $\varphi' \leftarrow \text{SwingTrajectoryEngine}(\mathbf{f}'_{\text{swg}}, \mathbf{f}''_{\text{sup}});$ 
10        if  $\varphi' \neq \emptyset$  then
11          | UpdateEdge( $\mathcal{T}, v', v'', \varphi'$ );
12        else
13          | RemoveSubtree( $\mathcal{T}, v''$ );
14        end
15      end
16    end
17  end
18 end
19 return;

```

Algorithm 2: SensorBasedFootstepPlanner

Input: $(\mathbf{f}^{j+1}_{\text{swg}}, \mathbf{f}^{j+1}_{\text{sup}}), \mathcal{G}, \Delta T^j, \mathcal{M}_z^j$
Output: $\mathcal{P}^{j+1,*}$

```

1  $(\mathcal{T}^{j+1}, v^{\text{root}}) \leftarrow \text{InitializeTree}(\mathcal{T}^j, (\mathbf{f}^{j+1}_{\text{swg}}, \mathbf{f}^{j+1}_{\text{sup}}));$ 
2  $\mathcal{V}_{\text{child}} \leftarrow \text{ChildVertexes}(\mathcal{T}^{j+1}, v^{\text{root}});$ 
3 foreach  $v' \in \mathcal{V}_{\text{child}}$  do
4   | UpdateTree( $\mathcal{T}^{j+1}, v', \mathcal{M}_z^j$ );
5 end
6 ExpandTree( $\mathcal{T}^{j+1}, \Delta T^j - \Delta T_e, \mathcal{M}_z^j$ );
7  $\mathcal{P}^{j+1,*} \leftarrow \text{RetrieveBestPlan}(\mathcal{T}^{j+1}, \mathcal{G});$ 
8 return  $\mathcal{P}^{j+1,*};$ 

```

Procedure 5: InitializeTree

Input: $\mathcal{T}^j, (\mathbf{f}^{j+1}_{\text{swg}}, \mathbf{f}^{j+1}_{\text{sup}})$
Output: $\mathcal{T}^{j+1}, v^{\text{root}}$

```

1  $v^{\text{root}} \leftarrow \text{NearestVertex}(\mathcal{T}^j, (\mathbf{f}^{j+1}_{\text{swg}}, \mathbf{f}^{j+1}_{\text{sup}}));$ 
2  $\mathcal{T}^{j+1} \leftarrow \text{ExtractSubtree}(\mathcal{T}^j, v^{\text{root}});$ 
3 UpdateVertex( $\mathcal{T}^{j+1}, v^{\text{root}}, (\mathbf{f}^{j+1}_{\text{swg}}, \mathbf{f}^{j+1}_{\text{sup}})$ );
4 return  $(\mathcal{T}^{j+1}, v^{\text{root}});$ 

```

Procedure 6: UpdateTree

Input: $\mathcal{T}^{j+1}, v, \mathcal{M}_z^j$

Output: none

```

1  $v^{\text{parent}} \leftarrow \text{ParentVertex}(\mathcal{T}^{j+1}, v);$ 
2  $z_{f,\text{sup}} \leftarrow \text{DetermineFootstepHeight}(\mathbf{f}_{\text{sup}}, \mathcal{M}_z^j);$ 
3  $\text{UpdateVertex}(\mathcal{T}^{j+1}, v, (\mathbf{f}_{\text{sup}}^{\text{parent}}, (x_{f,\text{sup}}, y_{f,\text{sup}}, z_{f,\text{sup}})));$ 
4 if R1( $\mathbf{f}_{\text{sup}}$ ) and R2( $\mathbf{f}_{\text{sup}}, \mathbf{f}_{\text{sup}}^{\text{parent}}$ ) then
5    $\varphi^{\text{parent}} \leftarrow \text{SwingTrajectoryEngine}(\mathbf{f}_{\text{swg}}^{\text{parent}}, \mathbf{f}_{\text{sup}});$ 
6   if R3( $\varphi^{\text{parent}}, (\mathbf{f}_{\text{swg}}, \mathbf{f}_{\text{sup}})$ ) then
7      $\text{UpdateEdge}(\mathcal{T}^{j+1}, v^{\text{parent}}, v, \varphi^{\text{parent}});$ 
8     if Depth( $\mathcal{T}^{j+1}, v)$ ) =  $\bar{\kappa}$  then
9       | return;
10      end
11       $\mathcal{V}_{\text{child}} \leftarrow \text{ChildVerteices}(\mathcal{T}^{j+1}, v);$ 
12      foreach  $v' \in \mathcal{V}_{\text{child}}$  do
13        |  $\text{UpdateTree}(\mathcal{T}^{j+1}, v', \mathcal{M}_z^j);$ 
14      end
15    else
16      |  $\text{RemoveSubtree}(\mathcal{T}^{j+1}, v);$ 
17    end
18  else
19    |  $\text{RemoveSubtree}(\mathcal{T}^{j+1}, v);$ 
20  end
21 return;

```

Chapter 4

Feasibility-aware plan adaptation in humanoid gait generation

4.1 Introduction

Humanoid robot locomotion is a complex task that involves multiple concurrent activities. It is usually tackled by breaking it down into several subproblems and solving each of them more or less independently. The first component is in general a footstep planner, which determines a sequence of footstep, e.g., leading the robot to some desired location. This sequence of footsteps must be kinematically realizable at least in terms of step lengths. The humanoid dynamics are usually accounted for in a second stage, typically based on Model Predictive Control (MPC), using a simplified robot model which is used to generate Center of Mass (CoM) trajectories. MPC, in its basic form, allows to perform real-time footstep position adaptation [29] and obtain reactive stepping so to reject pushes and impacts. However, in order to be able to formulate the optimization problem as a Quadratic Program (QP), constraints should be kept linear. For this reason, most schemes only adapt footstep positions, leaving out footstep orientation and step timing.

Several efforts to improve this basic paradigm have been made. To include automatic step timing adaptation, one could make the MPC nonlinear [30, 31, 32, 33], denying real-time implementation or requiring significant compromise in the control rate. A linear formulation is obtainable by considering only the duration of the first footstep [34, 35]. As for footstep orientation, this is also often ignored or planned independently of the dynamics [29]. To couple rotation decision with the dynamics, some schemes employ non-convex optimization through nonlinear [36, 37] or Mixed-Integer Programming (MIP) [30]. MIP can also be used to alternatively select between multiple convex regions in which to place the footsteps, which would otherwise constitute a non-convex constraint [38, 9].

Our architecture is based on the Intrinsically Stable MPC (IS-MPC) of [20], which involves an explicit stability constraint ensuring the boundedness of the CoM trajectory with respect to the ZMP and is recursive feasible. The feasibility region, i.e., the state space region for which the constrained QP admits a solution, can be used to enhance the scheme capabilities by adapting the timing of the first step [34], or to allow for non-convex regions [39] without burdening the optimization problem

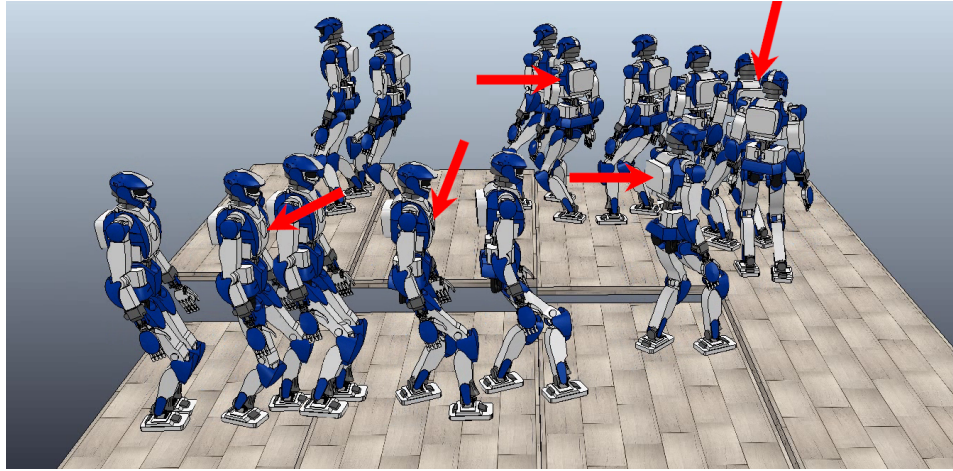


Figure 4.1. An example simulation using the proposed architecture: the robot is walking along a staircase while being subject to multiple pushes. The adaptation module modifies position, orientation and timing of the footsteps real-time to guarantee a successful execution.

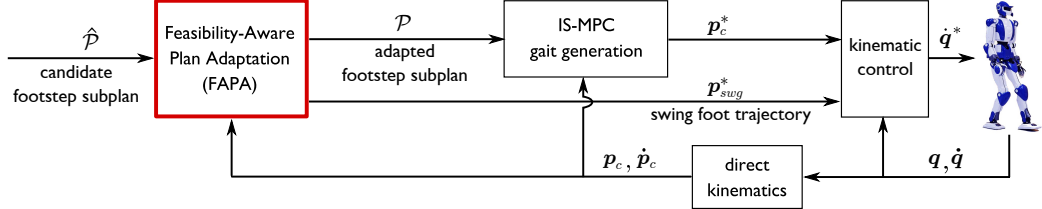


Figure 4.2. A block scheme of the proposed architecture. The candidate footstep subplan \hat{P} is adapted by the FAPA module, guaranteeing the feasibility of IS-MPC. The IS-MPC module receives the adapted footstep subplan P , and generates a desired trajectory of the CoM p_c^* , which is used by the kinematic controller, together with the desired trajectory of the swing foot p_{swg}^* , to generate the desired joint velocities \dot{q}^* .

of the MPC.

In this paper, we add an online adaptation module that can locally adapt footsteps (positions, timings and orientation) so to guarantee feasibility of the subsequent IS-MPC stage. The Feasibility-Aware Plan Adaptation (FAPA) is thus dependent on the system state and the dynamics of the chosen template dynamic model.

We obtain the generality given by nonlinear constraints without sacrificing much performance as the number of variables in the planner is much lower than that of the variables of the MPC, making it very fast and capable of working in real time. Furthermore, we explore the inclusion of integer variables, further increasing the range of situations that can be covered.

Modules for online footstep adaptation using nonlinear optimization have been proposed [40], but not in conjunction with MPC. Our approach is not only designed to work along with the MPC module, but it specifically aimed at enhancing its capabilities.

The remainder of the paper is organized as follows. Sect. 4.2 gives a general formulation of the problem. Sect. 4.3 introduces some preliminary notions. Sect. 4.4 details the MPC formulation. Sect. 4.5 describes both versions of the proposed FAPA: without and with integer variables. Sect. 4.6 shows and discusses some

simulations. Finally, Sect. 4.7 presents concluding remarks and future extensions.

4.2 Problem formulation

The proposed architecture is shown in Fig. 4.2. An external candidate plan is provided, which in this paper will be either a basic plan to demonstrate simple motions, or a plan generated by randomized exploration [41] for more complex environments. A subplan, i.e., a portion of the candidate plan, is given as input to the scheme at each timestep.

The basic components of the considered scheme are:

- a Feasibility-Aware Plan Adaptation (FAPA) block, that can modify locally the high-level footstep plan;
- an IS-MPC gait generation block that generates CoM/ZMP trajectories based on the output of FAPA;
- a kinematic controller that realizes at the joint level the generated CoM and swing foot trajectories.

While the high-level footstep plan is designed considering the humanoid’s kinematic limitations, it is entirely unaware of its dynamics and is not informed by the robot state since it is fully generated off-line. To make up for this deficiency, the FAPA module performs a local adaptation of the planned footsteps before these enter the IS-MPC stage.

This adaptation is based on a *gait feasibility constraint* that guarantees feasibility of the next IS-MPC stage while trying to match the original plan. It can concurrently change the footstep positions, orientations, as well as step timings.

To formulate this constraint, we leverage the feasibility region of IS-MPC, i.e., the subset of the state space where the problem is feasible at a given time. While in previous analyses we provided approximate closed-form expressions for these region bounds, here we rather define the feasibility region in an implicit form with the nonlinear dependency on the footstep positions, orientations, and step timings.

The fact that the feasibility of the MPC can be efficiently captured by the expression of this constraint is a crucial aspect of the formulation, because it means that the scheme can harness the power of nonlinear optimization without burdening the MPC itself, which remains linear and can run at a high rate. The nonlinear optimization part is external to the MPC, which allows the number of variables to be kept small and thus to keep the computation time manageable.

We propose two versions of the FAPA module, that differ by the optimization problem required for their implementation. In particular, the first version only uses continuous optimization, while the second one also employs discrete variables and is formulated as a Mixed Integer Nonlinear Program (MINLP). Being the latter very general it can be used to account for more adaptation scenarios, e.g., in which the footsteps can also be moved to different terrain patches than the ones assigned by the high-level planner. As will be discussed extensively in Sect. 4.6, the second version is more demanding in terms of computation time, but we present it as a proof of concept as we strongly believe it can be made to work in real time with proper code optimization.

4.3 Preliminaries

In this section we describe the environment and the structure of the footstep plan used in our scheme.

4.3.1 Environment

The considered environment is a world of stairs, i.e., constituted by flat horizontal regions. The robot is allowed to walk across different regions if these are relatively close in height, and if there is sufficient available surface to step on them, otherwise they will constitute obstacles to be avoided.

The arrangement of these regions is assumed to be known, and it is processed and encoded in the following way:

- regions are reduced in size so that they represent the collision-free area available for the center of the footprint. This is done by performing a Minkowski difference between each flat region and the area swept by a footprint (accounting for all possible footstep orientations);
- after reduction, non-convex regions are subdivided into non-overlapping convex polytopic *patches*.

A patch P is identified by the inequality $\mathbf{A}(P)\mathbf{p} \leq \mathbf{b}(P)$, where $\mathbf{A}(P) \in \mathbb{R}^{V(P) \times 2}$ and $\mathbf{b}(P) \in \mathbb{R}^{V(P)}$ define a polytope (with $V(P)$ vertices) and $\mathbf{p} = (x, y)^T$ is a generic 2D point. In this way, non-polytopic portions of ground (e.g., round edges) are approximated, but the number of vertices can be arbitrarily large. Since each patch P is flat, its height is denoted simply as $z(P)$.

4.3.2 Footstep plan

The high-level footstep plan is a sequence of *candidate footsteps* $\hat{\mathbf{f}}$, each identified by the tuple $\hat{\mathbf{f}} = (\hat{x}_f, \hat{y}_f, \hat{z}_f, \hat{\theta}_f, \hat{T}_{\text{ss}}, \hat{T}_{\text{ds}})$. For each planned footstep $\hat{\mathbf{f}}$

- \hat{x}_f , \hat{y}_f and \hat{z}_f are the coordinates of its center;
- $\hat{\theta}_f$ is its orientation around the z axis;
- \hat{T}_{ds} and \hat{T}_{ss} are the durations of its double support and single support phases, respectively;
- we denote by $\Pi(\hat{\mathbf{f}})$ the patch that contains the footstep, i.e., the patch P such that¹

$$(\hat{x}_f, \hat{y}_f)^T \in P, \quad \hat{z}_f = z(P).$$

The footstep plan $\hat{\mathcal{P}}$ is computed off-line, and at each time t_k a subplan $\hat{\mathcal{P}}^l$ of size $F+1$ is extracted, where l is the index of the first footstep of the current subplan (at t_k), and F a fixed parameter. The subplan contains the next F candidate footsteps:

$$\hat{\mathcal{P}}^l = \left\{ \hat{\mathbf{f}}^l, \dots, \hat{\mathbf{f}}^{l+F} \right\}.$$

¹Note that this patch is unique because the environment is subdivided into non-overlapping patches.

The FAPA block, which performs footsteps adaptation, modifies $\hat{\mathcal{P}}^l$ in the adapted subplan \mathcal{P}^l , i.e., in the input of the IS-MPC block

$$\mathcal{P}^l = \left\{ \mathbf{f}^l, \dots, \mathbf{f}^{l+F} \right\}.$$

After every iteration, if adaptation took place (i.e., \mathcal{P}^l differs from $\hat{\mathcal{P}}^l$), the algorithm performs a *footstep plan override*, i.e., the corresponding portion of the high-level footstep plan is substituted with the adapted subplan \mathcal{P}^l . Note that the remaining part of the plan (after the index $l + F$) is unchanged, so if the adaptation makes the robot stray from the initial path it will later try to catch up. This behavior is often acceptable, but might sometimes be undesirable, and can be improved in future versions if we allow the high-level planner to replan on-line (see [41]).

4.4 Gait generation via IS-MPC

We first illustrate the IS-MPC block in order to introduce concepts that are necessary to explain the FAPA block.

We describe the prediction model, the constraints, and the optimization problem to be solved. Furthermore, we give an expression for the feasibility region of IS-MPC in a suitable form to be used by the proposed scheme.

4.4.1 Prediction model

The prediction model is derived from balancing moments around the ZMP. To allow vertical motion of the CoM, some works [3] use the VH-IP model, in which height variations cause a change to the natural frequency of an inverted pendulum. This makes the prediction model nonlinear, negatively impacting performance. It is however possible to generate 3D trajectories using a linear model if we constrain the systems to obey the linear dynamics

$$\ddot{\mathbf{p}}_c = \eta^2(\mathbf{p}_c - \mathbf{p}_z) + \mathbf{g}, \quad (4.1)$$

as in [41], where $\mathbf{p}_c = (x_c, y_c, z_c)^T$ is the CoM position, $\mathbf{p}_z = (x_z, y_z, z_z)^T$ is the ZMP position, η is a design parameter² and $\mathbf{g} = (0, 0, -9.81)^T$ [m/s²] is the gravity acceleration vector. In order to have smoother trajectories, we dynamically extend (4.1) by having the derivative of the ZMP $\dot{\mathbf{p}}_z$, instead of the ZMP itself, be the input of the model.

Through the change of coordinates $\mathbf{p}_u = \mathbf{p}_c + \dot{\mathbf{p}}_c/\eta$, the dynamics of the unstable component (also *divergent component of motion* [42] or *capture point* [43]) can be highlighted:

$$\dot{\mathbf{p}}_u = \eta(\mathbf{p}_u - \mathbf{p}_z) + \mathbf{g}/\eta.$$

Despite this unstable dynamics, the CoM trajectory is bounded with respect to the ZMP if the following *stability condition* is satisfied:

$$\mathbf{p}_u^k = \eta \int_{t_k}^{\infty} e^{-\eta(\tau-t_k)} \mathbf{p}_z(\tau) d\tau - \frac{\mathbf{g}}{\eta}, \quad (4.2)$$

²The parameter η should be chosen by taking into account the desired resting height of the humanoid, because eq. (4.1) has an equilibrium when CoM and ZMP are vertically displaced by \mathbf{g}/η^2 .

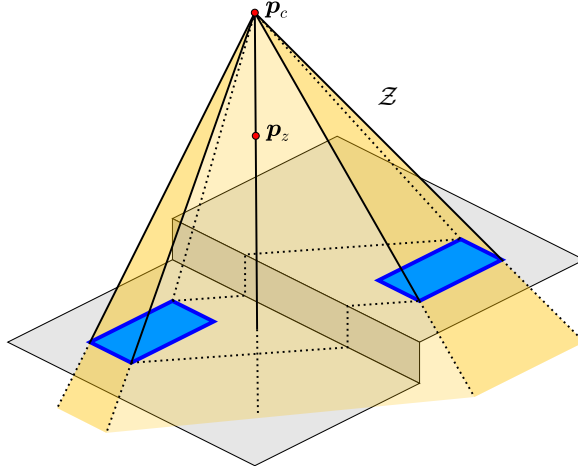


Figure 4.3. 3D balance: the ZMP \mathbf{p}_z must be inside the pyramid \mathcal{Z} .

where the superscript in \mathbf{p}_u^k indicates that the variable is sampled at time t_k .

The MPC module works over discrete time-steps of duration δ , over which the input $\dot{\mathbf{p}}_z$ is constant, i.e., $\dot{\mathbf{p}}_z(t) = \dot{\mathbf{p}}_z^k$ for $t \in [t_k, t_{k+1})$. The prediction model (4.1) is used to forecast the evolution of the system over a *control horizon* $T_c = C\delta$, while we assume to know the footstep plan over a *preview horizon* $T_p = P\delta$, with $P \geq C$.

Relating the dynamics of the CoM to those of the ZMP is essential since the latter encodes information about the realizability of ground reaction forces, and thus provides a criterion for balance. A common way to extend the basic 2D balance criterion consists in prescribing the 3D ZMP to be inside a 3D pyramid \mathcal{Z} (see Fig. 4.3), having the base defined by the contact surfaces and the CoM vertex [44, 41].

4.4.2 ZMP constraint

The IS-MPC block receives the adapted subplan \mathcal{P}^l and uses it to construct ZMP constraints. As described in the previous subsection, the criterion for balance is satisfied if the ZMP belongs to the pyramid \mathcal{Z} . However, enforcing this condition directly would lead to a nonlinear constraint in the MPC because the vertex of the pyramid is the CoM of the robot. Thus, we adopt a conservative approximation called the *moving constraint*.

The moving constraint requires for the ZMP to be at all times within a convex polyhedron of fixed shape, in our case a box of dimensions d_x , d_y and d_z centered in $\mathbf{p}_{mc} = (x_{mc}, y_{mc}, z_{mc})$, which we call the *moving box*. Along the prediction, the moving box can translate but not rotate, and its center moves in such a way that it is always fully contained within the 3D pyramid \mathcal{Z} (see Fig. 5 in [4]). The vector $\mathbf{X}_{mc}^{k+1} = (x_{mc}^{k+1}, \dots, x_{mc}^{k+C})^T$ collects the x coordinate of the center of the moving box in the control horizon.

Because of its constant orientation in the prediction, at each time we can choose the orientation of the axes to align with the orientation of the moving box (taken as the orientation of the current support foot) and obtain a ZMP constraint that is decoupled along the 3 axes. Focusing on the component along x , we can write it as

$$\mathbf{X}_z^{m,k+1} \leq \mathbf{X}_z^{k+1} \leq \mathbf{X}_z^{M,k+1}, \quad (4.3)$$

where $\mathbf{X}_z^{k+1} = (x_z^{k+1}, \dots, x_z^{k+C})^T$ is a vector of predicted ZMP positions, and $\mathbf{X}_z^{\text{m},k+1}$ and $\mathbf{X}_z^{\text{M},k+1}$ are the ZMP bounds along the prediction. By defining

$$\mathbf{Z} = \begin{pmatrix} \delta & 0 & \cdots & 0 \\ \delta & \delta & \cdots & 0 \\ \vdots & \vdots & \ddots & \vdots \\ \delta & \delta & \cdots & \delta \end{pmatrix}, \quad \mathbf{z} = \begin{pmatrix} 1 \\ 1 \\ \vdots \\ 1 \end{pmatrix},$$

\mathbf{X}_z^{k+1} can be expressed as

$$\mathbf{X}_z^{k+1} = \mathbf{Z} \dot{\mathbf{X}}_z^k + \mathbf{z} x_z^k, \quad (4.4)$$

where $\dot{\mathbf{X}}_z^k = (\dot{x}_z^k, \dots, \dot{x}_z^{k+C-1})^T$ is the vector of ZMP velocities, i.e., the decision variables. The ZMP bounds along the prediction can be expressed as

$$\mathbf{X}_z^{\text{m},k+1} = \mathbf{X}_{\text{mc}}^{k+1} - \mathbf{z} \frac{d_x}{2}, \quad \mathbf{X}_z^{\text{M},k+1} = \mathbf{X}_{\text{mc}}^{k+1} + \mathbf{z} \frac{d_x}{2}. \quad (4.5)$$

The center of the moving box \mathbf{p}_{mc} must be expressed in terms of the subplan \mathcal{P}^l . First we define the *piecewise-linear sigmoid* function

$$\sigma(t, t_i, t_f) = \frac{1}{t_f - t_i} (\rho(t - t_i) - \rho(t - t_f)),$$

where $\rho(t) = t\delta_{-1}(t)$ is the unit ramp. $\sigma(t, t_i, t_f)$ is 0 before t_i , 1 after t_f , and it transitions linearly in the interval $[t_i, t_f]$. This function is useful to represent the transition between consecutive footsteps.

$\mathbf{X}_{\text{mc}}^{k+1}$ can be written as

$$\mathbf{X}_{\text{mc}}^{k+1} = \mathbf{M} \mathbf{X}_f^l + \mathbf{m} x_f^l, \quad (4.6)$$

where $\mathbf{X}_f^l = (x_f^l, \dots, x_f^{l+F})^T$ collects the footstep positions. $\mathbf{M} \in \mathbb{R}^{C \times F}$ is a mapping matrix whose elements M_{ij} are defined as

$$M_{ij} = \sigma(t_{k+i}, t_s^{l+j}, t_s^{l+j} + T_{\text{ds}}^{l+j}) - \sigma(t_{k+i}, t_s^{l+j-1}, t_s^{l+j-1} + T_{\text{ds}}^{l+j-1}), \quad (4.7)$$

and $\mathbf{m} \in \mathbb{R}^C$ is a vector whose elements m_i are given by

$$m_i = 1 - \sigma(t_{k+i}, t_s^l, t_s^l + T_{\text{ds}}^l),$$

where t_s^l is the starting time of the l -th step and

$$t_s^j = t_s^l + \sum_{\lambda=l}^{l+j-1} (T_{\text{ds}}^\lambda + T_{\text{ss}}^\lambda).$$

4.4.3 Stability constraint

The stability constraint is derived from the stability condition (4.2). We focus here on the x component, but the other components can be similarly derived (see [41]).

Since the MPC has a limited control horizon we split the integral at t_{k+C} . Before t_{k+C} the stability condition can be expressed in terms of the decision variables, while after it must be conjectured. We adopt the anticipative tail \tilde{x}_z [20] to get an approximation of the ZMP trajectory after the horizon:

$$\eta \int_{t_k}^{t_{k+C}} e^{-\eta(\tau-t_k)} x_z(\tau) d\tau = x_u^k - \tilde{c}_x^k,$$

where x_u^k is the x -component of \mathbf{p}_u^k and

$$\tilde{c}_x^k = \eta \int_{t_{k+C}}^{\infty} e^{-\eta(\tau-t_k)} \tilde{x}_z(\tau) d\tau.$$

The second step is to make the decision variables appear explicitly, i.e., the ZMP velocities $\dot{\mathbf{X}}_z$ over the control horizon, by computing the integral over a piecewise linear ZMP trajectory. The final form of the constraint can be found in [20]. For the purpose of this analysis, we will use the compact expression

$$\mathbf{s}^T \dot{\mathbf{X}}_z = b_x^k + x_u^k, \quad (4.8)$$

where $\mathbf{s} \in \mathbb{R}^C$ and $b_x^k \in \mathbb{R}$ denote respectively a vector and a scalar whose explicit expressions can be recovered from the cited reference.

4.4.4 IS-MPC algorithm

IS-MPC solves, at each time t_k , the following QP problem:

$$\left\{ \begin{array}{l} \min_{\dot{\mathbf{X}}_z^k, \dot{\mathbf{Y}}_z^k, \dot{\mathbf{Z}}_z^k} \|\dot{\mathbf{X}}_z^k\|^2 + \|\dot{\mathbf{Y}}_z^k\|^2 + \|\dot{\mathbf{Z}}_z^k\|^2 + \beta \|\mathbf{X}_z^{k+1} - \mathbf{X}_{mc}^{k+1}\|^2 \\ \quad + \beta \|\mathbf{Y}_z^{k+1} - \mathbf{Y}_{mc}^{k+1}\|^2 + \beta \|\mathbf{Z}_z^{k+1} - \mathbf{Z}_{mc}^{k+1}\|^2 \\ \text{subject to:} \\ \bullet \text{ ZMP constraints (4.3)} \\ \bullet \text{ stability constraints (4.8)} \end{array} \right.$$

In the cost function, the first three terms act as regularization while the remaining attempt to bring the ZMP as close as possible to the center of the moving box, with a strength modulated by the weight β .

The first sample $\dot{\mathbf{p}}_z^k = (\dot{x}_z^k, \dot{y}_z^k, \dot{z}_z^k)$ of the optimal sequence is used to integrate the prediction model and the resulting CoM position \mathbf{p}_c^{k+1} is sent to the kinematic controller together with a suitable swing foot trajectory that allows to reach the target footstep position at the proper time.

4.4.5 Feasibility region

The *feasibility region* is the region of the state space in which the IS-MPC optimization problem is feasible.

Proposition 1 IS-MPC is feasible at time t_k if

$$\begin{aligned} \mathbf{s}^T \mathbf{Z}^{-1}(\mathbf{X}_z^{m,k+1} - \mathbf{z}x_z^k) &\leq x_u^k + b_x^k \leq \mathbf{s}^T \mathbf{Z}^{-1}(\mathbf{X}_z^{M,k+1} - \mathbf{z}x_z^k), \\ \mathbf{s}^T \mathbf{Z}^{-1}(\mathbf{Y}_z^{m,k+1} - \mathbf{z}y_z^k) &\leq y_u^k + b_y^k \leq \mathbf{s}^T \mathbf{Z}^{-1}(\mathbf{Y}_z^{M,k+1} - \mathbf{z}y_z^k), \\ \mathbf{s}^T \mathbf{Z}^{-1}(\mathbf{Z}_z^{m,k+1} - \mathbf{z}z_z^k) &\leq z_u^k + b_z^k \leq \mathbf{s}^T \mathbf{Z}^{-1}(\mathbf{Z}_z^{M,k+1} - \mathbf{z}z_z^k). \end{aligned} \quad (4.9)$$

Proof. We focus the proof on the inequalities for the x component, as the logic, for the other components is identical. The bounds of the feasibility region along x are given by

$$\begin{aligned} x_u^{k,b1} &= \mathbf{s}^T \mathbf{Z}^{-1}(\mathbf{X}_z^{m,k+1} - \mathbf{z}x_z^k) - b_x^k, \\ x_u^{k,b2} &= \mathbf{s}^T \mathbf{Z}^{-1}(\mathbf{X}_z^{M,k+1} - \mathbf{z}x_z^k) - b_x^k. \end{aligned}$$

Then, if x_u^k is inside the feasibility region, it is possible to express it as a convex combination of the two bounds, i.e.,

$$x_u^k = \alpha x_u^{k,b1} + (1 - \alpha)x_u^{k,b2}, \alpha \in [0, 1]. \quad (4.10)$$

Consider the following ZMP velocity trajectory:

$$\dot{\mathbf{X}}_z^k = \alpha \mathbf{Z}^{-1}(\mathbf{X}_z^{m,k+1} - \mathbf{z}x_z^k) + (1 - \alpha) \mathbf{Z}^{-1}(\mathbf{X}_z^{M,k+1} - \mathbf{z}x_z^k). \quad (4.11)$$

We will show that this particular trajectory satisfies both the stability constraint and the ZMP constraints. As for the stability constraint, multiply both sides of (4.11) by \mathbf{s}^T and plug in the definitions of $x_u^{k,b1}$ and $x_u^{k,b2}$ to obtain

$$\mathbf{s}^T \dot{\mathbf{X}}_z^k = (\alpha(x_u^{k,b1} + b_x^k)) + (1 - \alpha)(x_u^{k,b2} + b_x^k).$$

Using (4.10), this is equivalent to the stability constraint (4.8).

To prove satisfaction of the ZMP constraint. Left-multiplying (4.4) by \mathbf{Z} , the chosen ZMP velocity trajectory can be rewritten as

$$\mathbf{X}_z^k - \mathbf{z}x_z^k = \alpha(\mathbf{X}_z^{m,k+1} - \mathbf{z}x_z^k) + (1 - \alpha)(\mathbf{X}_z^{M,k+1} - \mathbf{z}x_z^k),$$

which simplifies to $\mathbf{X}_z^k = \alpha \mathbf{X}_z^{m,k+1} + (1 - \alpha) \mathbf{X}_z^{M,k+1}$, and therefore the ZMP constraint (4.3) is satisfied. ■

In the following section, we will describe how to use the feasibility region to formulate a constraint for the FAPA module, and thus ensure that the output of FAPA can be used by IS-MPC to construct a feasible QP.

4.5 Feasibility-Aware Plan Adaptation

The FAPA module runs in real-time and performs a local adaptation of the subplan $\hat{\mathcal{P}}^l$, including their timing. We now describe the constraints and the optimization problems that define the adaptation procedure.

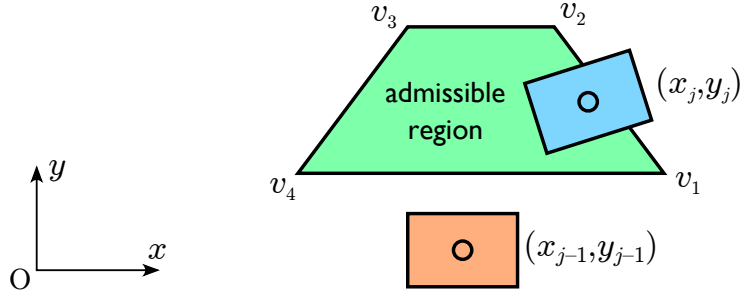


Figure 4.4. Admissible region of the kinematic constraint in the x - y plane.

4.5.1 Kinematic constraint

The j -th footstep \mathbf{f}^j is ensured to be kinematically feasible by limiting its displacement with respect to the previous footstep \mathbf{f}^{j-1} . In practice we constrain the geometric components of \mathbf{f}^j to be within the *admissible region*

$$\begin{pmatrix} \mathbf{n}_1^T (\mathbf{p}_{xy}^{l+j} - \mathbf{p}_{xy}^{l+j-1} - \mathbf{R}(\theta_f^{l+j-1})\mathbf{v}_1) \\ \vdots \\ \mathbf{n}_V^T (\mathbf{p}_{xy}^{l+j} - \mathbf{p}_{xy}^{l+j-1} - \mathbf{R}(\theta_f^{l+j-1})\mathbf{v}_V) \end{pmatrix} \geq \mathbf{0}, \quad (4.12)$$

$$\Delta z^m \leq z_{l+j} - z_{l+j-1} \leq \Delta z^M,$$

$$\Delta \theta^m \leq \theta_{l+j} - \theta_{l+j-1} \leq \Delta \theta^M,$$

with $\mathbf{R}(\theta_f^{l+j-1})$ a 2D rotation matrix, \mathbf{n}_i the vector normal to the i -th segment of the convex region computed as

$$\mathbf{n}_i = \begin{pmatrix} 0 & -1 \\ 1 & 0 \end{pmatrix} \mathbf{R}(\theta_f^{l+j-1})(\mathbf{v}_{i+1} - \mathbf{v}_i),$$

and \mathbf{v}_i being the vertices defining the convex polygon (different depending whether the support foot is left or right), shown in Fig. 4.4. Furthermore, Δz^m , Δz^M , $\Delta \theta^m$, and $\Delta \theta^M$ define limits for the foot reachability over vertical displacement and relative orientation.

4.5.2 Timing constraint

Single and double support duration are subject to minimum and maximum duration constraints

$$T_{ds}^{\min} \leq T_{ss}^{l+j} \leq T_{ds}^{\max}, \quad T_{ss}^{\min} \leq T_{ds}^{l+j} \leq T_{ss}^{\max}, \quad (4.13)$$

where the bounds T_{ds}^{\min} , T_{ds}^{\max} , T_{ss}^{\min} , T_{ss}^{\max} are chosen in such a way to avoid excessively fast trajectories that might be difficult to track, as well as very slow steps that could result in quasi-static motion.

4.5.3 Patch constraints

We describe alternative versions of this constraint, as we will later compare the module using either of them, both in terms of the quality of the resulting plan and of the computational load. The first version of the constraint simply restrict

the $(l + j)$ -th footstep to lie within its associated patch $\Pi(\mathbf{f}^{l+j})$, which is the one originally chosen by the high-level planner. This constraint can be written as

$$\begin{cases} \mathbf{A}(\Pi(\mathbf{f}^{l+j})) \begin{pmatrix} x_f^{l+j} & y_f^{l+j} \end{pmatrix}^T \leq \mathbf{b}(\Pi(\mathbf{f}^{l+j})), \\ z_f^{l+j} = z(\Pi(\mathbf{f}^{l+j})). \end{cases} \quad (4.14)$$

The second version of the patch constraint allows the footstep to be moved to a different patch. To entertain this possibility, we introduce binary variables in order to formulate a mixed-integer constraint. This constraint defines a logical implication in which, if a certain binary variable $b_{l+j,\kappa}$ is *true*, then a linear constraint must be verified:

$$b_{l+j,\kappa} = 1 \Rightarrow \begin{cases} \mathbf{A}(P^\kappa) \begin{pmatrix} x_f^{l+j} & y_f^{l+j} \end{pmatrix}^T \leq \mathbf{b}(P^\kappa), \\ z_f^{l+j} = z(P^\kappa). \end{cases} \quad (4.15)$$

This forces the $(l + j)$ -th footstep to lie within the κ -th patch. Since each footstep can only be inside a single patch, we also impose

$$\sum_{\kappa=1}^R b_{l+j,\kappa} = 1. \quad (4.16)$$

In MIP, logical implications can be implemented using binary variables through the so-called *big-M* technique [45]. In this case, we rewrite (4.15) as

$$\begin{cases} \mathbf{A}(P^\kappa) \begin{pmatrix} x_f^{l+j} & y_f^{l+j} \end{pmatrix}^T \leq \mathbf{b}(P^\kappa) + (1 - b_{l+j,\kappa})M\mathbf{1}_{V(P^\kappa)}, \\ z_{l+j} \leq z(P^\kappa) + (1 - b_{l+j,\kappa})M, \\ -z_{l+j} \leq -z(P^\kappa) + (1 - b_{l+j,\kappa})M, \end{cases} \quad (4.17)$$

where M is a constant large enough to relax the constraints if $b_{l+j,\kappa} = 0$ and $\mathbf{1}_{V(P^\kappa)}$ is a row vector with $V(P^\kappa)$ ones. We define $\hat{\kappa}_{l+j}$ as the index of $\Pi(\hat{\mathbf{f}}^{l+j})$. Note that this requires turning the equality constraint into two inequality constraints. Based on the patches of the candidate footsteps in $\hat{\mathcal{P}}^l$, we also define candidate binary variables as

$$\hat{b}_{l+j,\kappa} = \begin{cases} 1, & \text{if } \kappa = \hat{\kappa}_{l+j}, \\ 0, & \text{if } \kappa \neq \hat{\kappa}_{l+j}. \end{cases}$$

Finally, (4.16) and (4.17) assume that every footstep may be mapped to every patch, which requires $F \times R$ binary variables. However, since the computational load of a MIP is largely related to the number of binary variables, we employ a heuristic that allows a footstep \mathbf{f}^j to be assigned only to the patches adjacent to $\Pi(\hat{\mathbf{f}}^j)$.

4.5.4 Current footstep constraints

The first footstep in the subplan \mathbf{f}^l corresponds to the footstep currently in contact with the ground, which means that some of its components cannot be changed. In particular, its geometric components should be constrained to be equal to the corresponding components of $\hat{\mathbf{f}}^l$, i.e.,

$$x_f^l = \hat{x}_f^l, \quad y_f^l = \hat{y}_f^l, \quad z_f^l = \hat{z}_f^l, \quad \theta_f^l = \hat{\theta}_f^l. \quad (4.18)$$

Note that, because of the footstep plan override, the components of $\hat{\mathbf{f}}^l$ are not the same as in the original plan, but rather those adapted at the previous iteration.

If t_k belongs to a single support phase, the double support of the current step cannot be changed anymore because it is already passed. This is expressed by the constraint

$$t_k - t_s^l > T_{\text{ds}}^l \Rightarrow T_{\text{ds}}^l = \hat{T}_{\text{ds}}^l. \quad (4.19)$$

Note that the implication in (4.19) is handled at the code level and does not require introducing binary variables.

To avoid footstep changes when the swing foot is close to touching the ground, when nearing the end we add the following constraint:

$$T_{\text{ds}}^l + T_{\text{ss}}^l - t_k + t_s^l < t_{\text{change}} \Rightarrow \mathbf{f}^{l+1} = \hat{\mathbf{f}}^{l+1}. \quad (4.20)$$

4.5.5 Gait feasibility constraints

The gait feasibility constraints are introduced to ensure that IS-MPC is feasible. They do so by constraining the current state to be within the feasibility region (4.9).

The expression of the feasibility region (4.9) uses the ZMP bounds, that clearly depend on the motion of the moving box, and thus on the footsteps positions and timings. To derive a constraint, we simply make this dependency explicit by plugging (4.5) and (4.6) inside (4.9). Focusing on the right inequality of the x component, this results in

$$x_u^k + b_x^k \leq \mathbf{s}^T \mathbf{Z}^{-1} \left(\mathbf{M} \mathbf{X}_f^l + \mathbf{m} x_f^l + \mathbf{z} \left(\frac{d_x}{2} - x_z^k \right) \right). \quad (4.21)$$

The y and z components, as well as the left inequalities result in analogous expressions, which we omit for space concerns.

4.5.6 Feasibility-driven plan adaptation algorithm

We present two different versions of the FAPA algorithm. The first one is not allowed to move footsteps from a different patch to the one in the original plan, and is thus referred to as Fixed patches FAPA (F-FAPA). The second one is instead allowed to choose different patches, and goes under the name of Variables patches FAPA (V-FAPA).

The decision variable over the planning horizon are collected as

$$\begin{aligned} \mathbf{X}_f^l &= (x_f^l, \dots, x_f^{l+F}), & \mathbf{Y}_f^l &= (y_f^l, \dots, y_f^{l+F}), \\ \mathbf{Z}_f^l &= (z_f^l, \dots, z_f^{l+F}), & \Theta_f^l &= (\theta_f^l, \dots, \theta_f^{l+F}), \\ \mathbf{T}_{\text{ds}}^l &= (T_{\text{ds}}^l, \dots, T_{\text{ds}}^{l+F}), & \mathbf{T}_{\text{ss}}^l &= (T_{\text{ss}}^l, \dots, T_{\text{ss}}^{l+F}), \end{aligned}$$

$$\mathbf{B}^l = \begin{pmatrix} b_{l,1} & \dots & b_{l,L} \\ \vdots & \ddots & \vdots \\ b_{l+F,1} & \dots & b_{l+F,L} \end{pmatrix},$$

while the corresponding candidate values are identified by the vectors $\hat{\mathbf{X}}_f^l$, $\hat{\mathbf{Y}}_f^l$, $\hat{\mathbf{Z}}_f^l$, $\hat{\Theta}_f^l$, $\hat{\mathbf{T}}_{\text{ds}}^l$, $\hat{\mathbf{T}}_{\text{ss}}^l$, $\hat{\mathbf{B}}^l$, similarly defined.

F-FAPA solves the following problem, with decision variables $\mathbf{U}^l = (\mathbf{X}_f^l, \mathbf{Y}_f^l, \mathbf{Z}_f^l, \boldsymbol{\Theta}_f^l, \mathbf{T}_{ds}^l, \mathbf{T}_{ss}^l)$:

$$\left\{ \begin{array}{l} \min_{\mathbf{U}^l} w_x \|\hat{\mathbf{X}}_f^l - \mathbf{X}_f^l\|_2^2 + w_y \|\hat{\mathbf{Y}}_f^l - \mathbf{Y}_f^l\|_2^2 + \\ w_z \|\hat{\mathbf{Z}}_f^l - \mathbf{Z}_f^l\|_2^2 + w_\theta \|\hat{\boldsymbol{\Theta}}_f^l - \boldsymbol{\Theta}_f^l\|_2^2 + \\ w_{ds} \|\hat{\mathbf{T}}_{ds}^l - \mathbf{T}_{ds}^l\|_2^2 + w_{ss} \|\hat{\mathbf{T}}_{ss}^l - \mathbf{T}_{ss}^l\|_2^2 \end{array} \right.$$

subject to:

- kinematic constraints (4.12), for $j = 1, \dots, F$
- timing constraints (4.13), for $j = 0, \dots, F$
- fixed patch constraints (4.14), for $j = 1, \dots, F$
- current footsteps constraints (4.18), (4.19) and (4.20)
- gait feasibility constraints (4.21)

Since F-FAPA does not have binary variables, it can be implemented using a regular nonlinear solver (i.e., **ipopt**).

V-FAPA solves the following problem, with decision variables which now include the binary variables \mathbf{B}^l that is $\mathbf{W}^l = (\mathbf{X}_f^l, \mathbf{Y}_f^l, \mathbf{Z}_f^l, \boldsymbol{\Theta}_f^l, \mathbf{T}_{ds}^l, \mathbf{T}_{ss}^l, \mathbf{B}^l)$:

$$\left\{ \begin{array}{l} \min_{\mathbf{W}^l} w_x \|\hat{\mathbf{X}}_f^l - \mathbf{X}_f^l\|_2^2 + w_y \|\hat{\mathbf{Y}}_f^l - \mathbf{Y}_f^l\|_2^2 + \\ w_z \|\hat{\mathbf{Z}}_f^l - \mathbf{Z}_f^l\|_2^2 + w_\theta \|\hat{\boldsymbol{\Theta}}_f^l - \boldsymbol{\Theta}_f^l\|_2^2 + \\ w_{ds} \|\hat{\mathbf{T}}_{ds}^l - \mathbf{T}_{ds}^l\|_2^2 + w_{ss} \|\hat{\mathbf{T}}_{ss}^l - \mathbf{T}_{ss}^l\|_2^2 + \\ w_b \|\hat{\mathbf{B}}^l - \mathbf{B}^l\|_2^2 \end{array} \right.$$

subject to:

- kinematic constraints (4.12), for $j = 1, \dots, F$
- timing constraints (4.13), for $j = 0, \dots, F$
- variable patch constraints (4.16) and (4.17), for $j = 1, \dots, F$
- current footsteps constraints (4.18), (4.19) and (4.20)
- gait feasibility constraints (4.21)

Since V-FAPA contains the binary variables \mathbf{B} it is implemented as a MINLP.

4.6 Simulations

We ran four simulations in MATLAB, using CoppeliaSim to kinematically visualize the resulting motions. The system is an AMD Ryzen 9 5900X (4.8 GHz, 12 core) with 16 GB DDR4 3600 MHz running Ubuntu 22.04 LTS. IS-MPC runs at 100 Hz and is solved using quadprog, while FAPA runs at 10 Hz and is solved using the

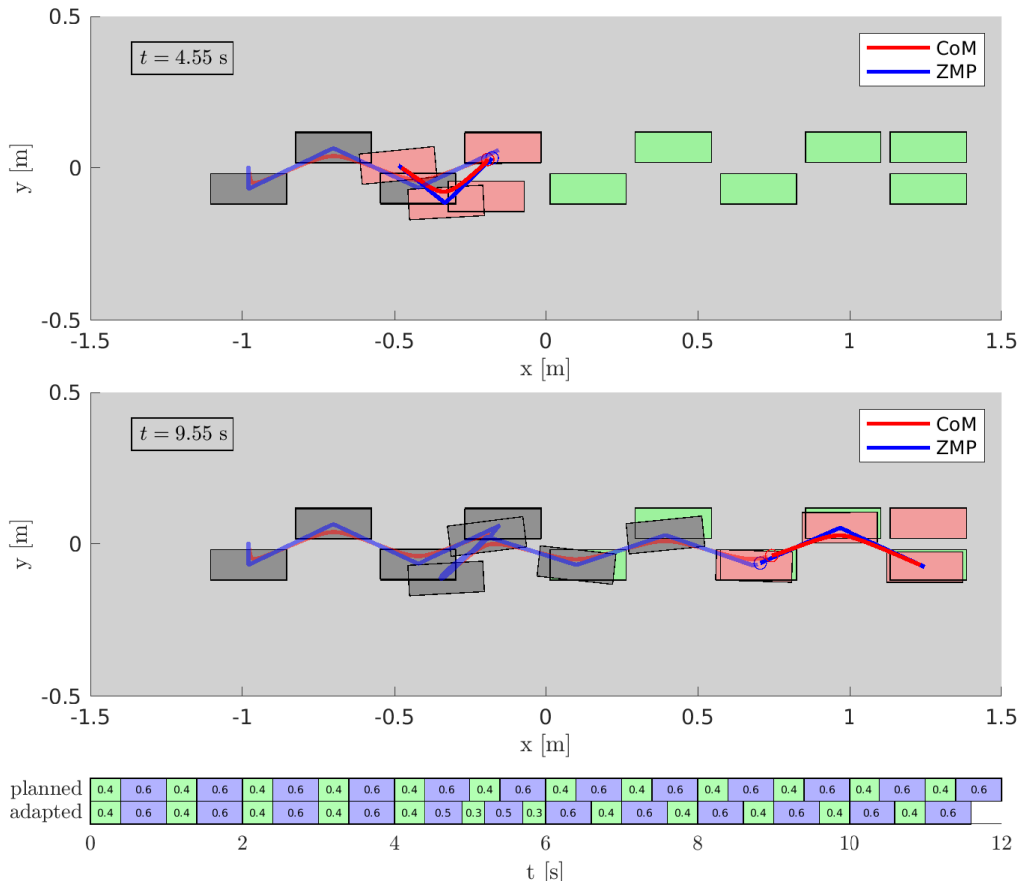


Figure 4.5. F-FAPA in the *empty* scenario. The robot is walking in a straight line and is pushed at time 4.5 s (slightly before the first snapshot). Green footsteps represent the original candidate plan, while the footsteps that are actually executed are shown in grey. Red footsteps represent the current adapted subplan. The two bands on the bottom show the nominal and adapted timings (green for double support and blue for single support). The same color scheme is used for the rest of the figures.

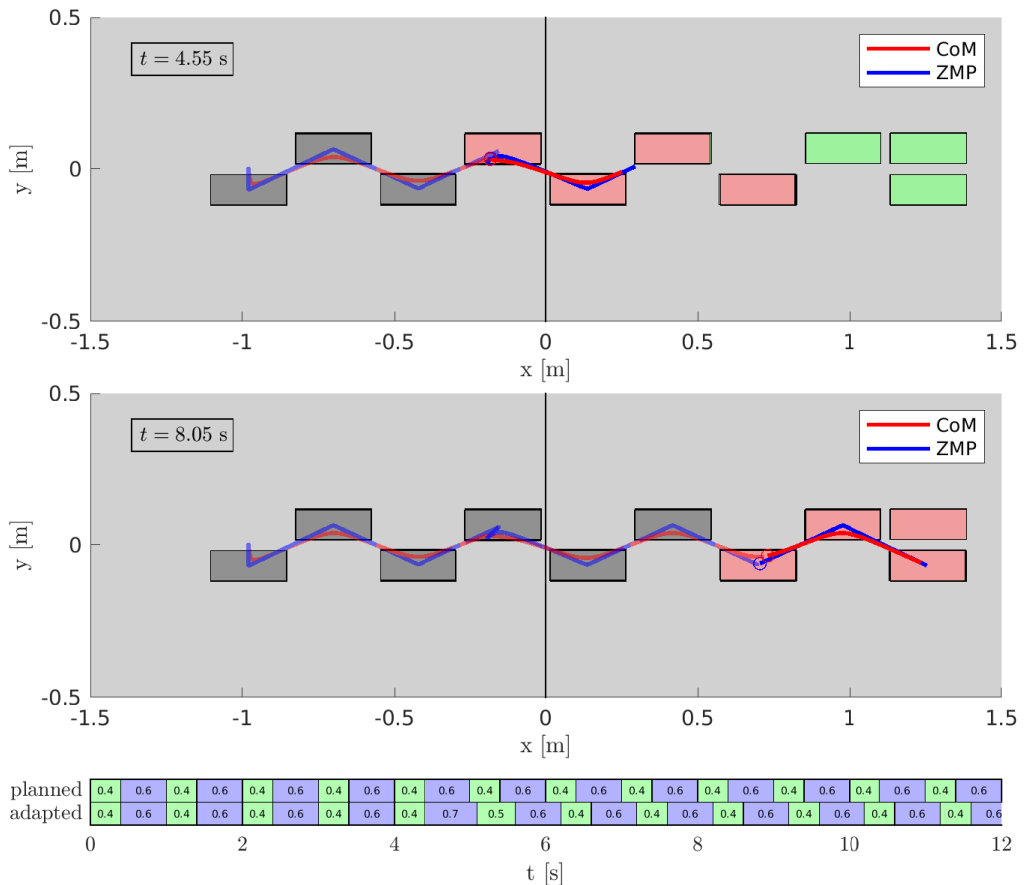


Figure 4.6. F-FAPA in the *2-patches* scenario. The robot is walking in a straight line and is pushed at time 4.5 s (slightly before the first snapshot). Since changing patches is not allowed, the magnitude of the push that can be tolerated is quite small, compared to that of the other simulations.

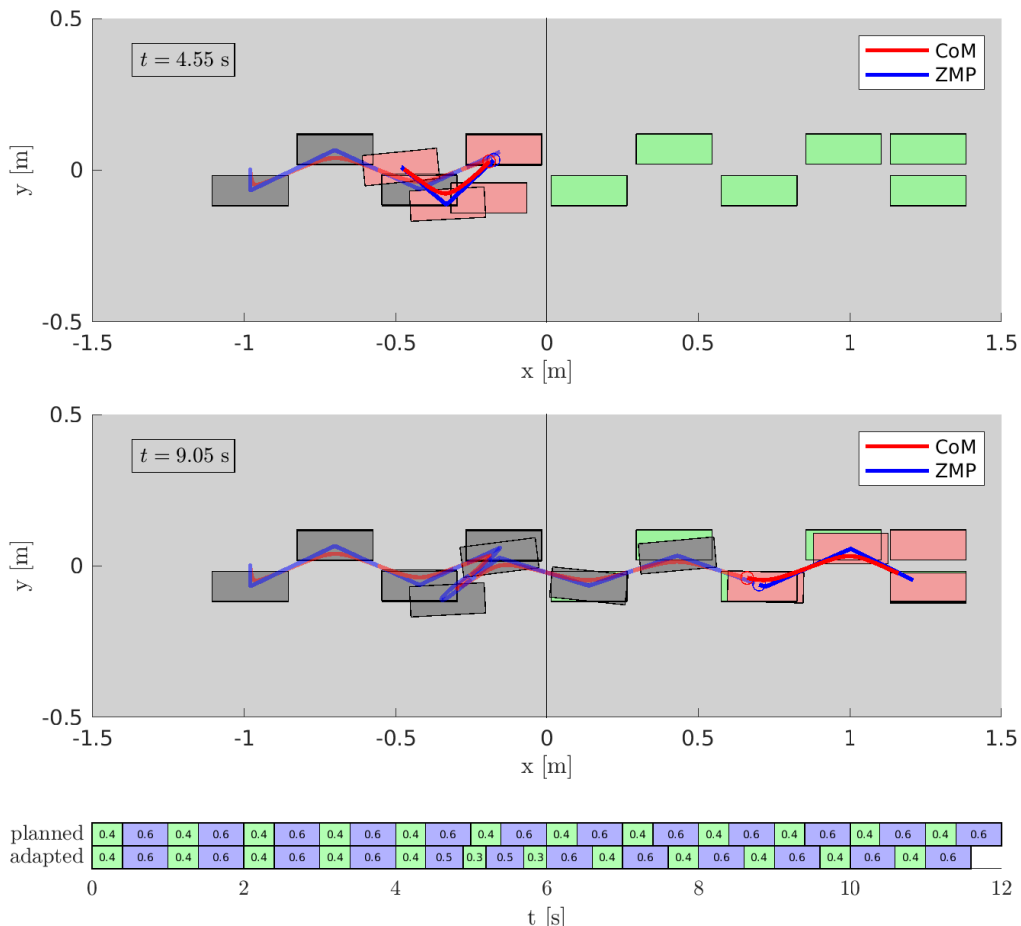


Figure 4.7. V-FAPA in the *2-patches* scenario. The robot is walking in a straight line and is pushed at time 4.5 s (slightly before the first snapshot). Now the robot is allowed to adapt the footstep position to the other patch, and is able to tolerate a stronger push.

Algorithm	Solver	Average [s]	Std dev. [s]	Max [s]
F-FAPA	<code>ipopt</code>	0.0207	0.0041	0.0467
F-FAPA	<code>knitro</code>	0.0144	0.0032	0.0329
V-FAPA	<code>bonmin</code>	0.3164	0.2075	1.2098
V-FAPA	<code>knitro</code>	0.0316	0.0393	0.3985

Table 4.1. Performance metrics of F-FAPA in the *empty* scenario and V-FAPA in the *2-patches* scenario, using different solvers.

CasADi interface. In CasADi, we used `ipopt` for F-FAPA, and `bonmin` for V-FAPA. We also ran tests with the commercial solver `knitro`, to compare the performance (see Table 4.1).

All the simulations use the following parameters: $\delta = 0.01$ s, $T_c = 2.0$ s, $T_p = 4.0$ s, $\eta = 3.6$ s $^{-1}$, $\beta = 100$, the size of the moving box are $d_x = d_y = d_z = 0.035$ m, $F = 3$, $\mathbf{v}_1 = (0.28, 0.13)^T$ m, $\mathbf{v}_2 = (0.2, 0.43)^T$ m, $\mathbf{v}_3 = (-0.12, 0.43)^T$ m, $\mathbf{v}_4 = (-0.2, 0.13)^T$ m, $\Delta_z^m = -0.10$ m, $\Delta_z^M = 0.10$ m, $\Delta_\theta^m = -0.4$ rad, $\Delta_\theta^M = 0.4$ rad, $T_{ds}^{\min} = 0.3$ s, $T_{ds}^{\max} = 0.5$ s, $T_{ss}^{\min} = 0.5$ s, $T_{ss}^{\max} = 0.7$ s, $t_{\text{change}} = 0.1$ s, $M = 100$, $w_x = w_y = w_z = w_\theta = w_{ds} = w_{ss} = 1.0$ and $w_b = 0.01$. Simulation videos are available at https://youtu.be/4_QYsZH1E7Y.

Simulations take place in 3 different scenarios: *empty*, which is completely flat with no obstacles, and is represented using a single patch; *2-patches* is constituted by two patches at different heights (0 and 0.06 m); *stairs* has a total of 7 patches of increasing height. While walking, the robot is subject to impulsive pushes (lasting 0.01 s), transformed in equivalent acceleration imparted on the Com.

In the first simulation, the robot is walking forward in the *empty* scenario. At 4.5 s it receives a 15.6 m/s 2 push in the direction $(-2, -1, 0)$, that without FAPA would make the MPC infeasible. F-FAPA reacts by adapting footstep positions, orientations and timings concurrently, allowing the MPC to recover feasibility. Figure 4.5 shows nominal and adapted footsteps, trajectories and step timings.

In the second simulation (shown in Fig. 4.6), the scenario is *2-patches*, and the robot must climb a step. Upon receiving the push, the footsteps do not change significantly, because the F-FAPA algorithm is not allowed to move the footstep to the other patch. As a result, the tolerable push is smaller, i.e., 7.8 m/s 2 .

In the third simulation (shown in Fig. 4.7), the scenario is still *2-patches*, but now the scheme is using V-FAPA. When the push is perceived, the first predicted footstep is moved to the lower patch, and as a result the increase of the tolerable push intensity is very significant, i.e., the same as in the *empty* scenario.

In the last simulation, the robot is moving through a more complex environment constituted by a long staircase. While climbing, the robot is subject to multiple pushes, triggering several footstep adjustments. Figure 4.1 shows a stroboscopic view of the motion.

To discuss the real-time applicability of the scheme, we report performance metrics in Table 4.1. The solvers used are `ipopt` and `knitro` for F-FAPA, and `bonmin` and `knitro` for V-FAPA. `knitro` is faster overall, but `ipopt` still demonstrates good performance for F-FAPA, compatible with real-time requirements. For V-FAPA, `bonmin` is clearly too slow, while `knitro` has an average performance that is real-time on average, but some outliers violate the requirements. Since all results in this paper are simulated, real-time performance is desirable but not critical. However, it is necessary for hardware implementation, which is why we will be working to

guarantee real-time performance in future works.

4.7 Conclusions

We presented a module for adapting positions, orientations and timings in such a way to enhance our IS-MPC scheme, using a gait feasibility constraint. Simulated results show that the plan is adapted in a very flexible way in reaction to strong pushes. In our MATLAB prototype, the performance is fully compatible with real time in the case of F-FAPA, while not yet in the case of V-FAPA. We believe that an optimized C++ implementation will be able to meet real-time requirements. Future work will be aimed at fully accommodating these requirements, as well as including the high-level planner [41] inside the architecture so that global replanning is possible.

Chapter 5

Nonlinear model predictive control for steerable wheeled mobile robots

Todo.

Chapter 6

Conclusions

Todo.

Appendix A

Gait generation via IS-MPC

A.1 Gait generation via IS-MPC (from WoS)

The gait generation module receives the planned footstep sequence \mathcal{S}_f as input, and it is in charge of producing a CoM trajectory that the robot can safely track in order to step over said footstep sequence. Along the entire motion, dynamic balance must be maintained.

On flat ground, it is common to ensure dynamic balance as a geometric criterion, by requiring that the ZMP must always be inside the convex hull of contact surfaces, i.e., the *support polygon*. Traditionally, the ZMP is assumed to be located on the ground plane, which is uniquely defined when the environment is flat.

In non-flat environments, there is no unique ground surface on which the ZMP can be assumed to be. However, the aforementioned criterion can be extended to these cases by allowing the ZMP to move in 3D [2]. The balance criterion is satisfied as long as the ZMP is inside a three-dimensional *support region* \mathcal{Z} that takes the shape of a pyramid (see Fig. A.1). The vertex of this pyramid is the robot CoM, and the edges are the lines connecting the CoM to the vertexes of the convex hull of the contact surfaces.

In MPC, dynamic balance is enforced via constraints on the ZMP position. However, the 3D support region \mathcal{Z} cannot be directly employed to enforce a ZMP constraint, because this would be nonlinear, meaning that the resulting optimization problem would not be in a standard linear-quadratic formulation. The cause of this nonlinearity is given by the fact that the vertex of the pyramid \mathcal{Z} is the CoM. Since both the ZMP and the CoM depend on the decision variables of the QP, this would result in product between the decision variables themselves.

In order to avoid this, we will define a smaller region, independent of the CoM position, where the ZMP is allowed to be. Furthermore, we will prove that this region conservatively approximates the actual support region \mathcal{Z} , and thus that the balance condition is always satisfied under the imposed constraints.

In this section we will describe the MPC gait generation scheme that is used in the proposed formulation. In particular, we will derive the prediction model and define the constraints that ensure stability and dynamic balance. Finally, we will state the QP problem to be solved at each iteration, and give a sketch of the complete algorithm.

A.1.1 Prediction Model

Control of the ZMP is achieved using a dynamic model relating the position of the latter to the position and acceleration of the CoM. This dynamic model can be derived by balancing moments on the humanoid as a whole, and assuming that the rate of change of angular momentum around the CoM can be neglected. With this in mind, denoting the CoM as $\mathbf{p}_c = (x_c, y_c, z_c)$ and the ZMP as $\mathbf{p}_z = (x_z, y_z, z_z)$, we get

$$\begin{aligned}(z_c - z_z)\ddot{x}_c &= (x_c - x_z)(\ddot{z}_c - g) \\ (z_c - z_z)\ddot{y}_c &= (y_c - y_z)(\ddot{z}_c - g),\end{aligned}\tag{A.1}$$

where g is the gravity acceleration.

This model exhibits a nonlinear coupling between the vertical and the horizontal components of \mathbf{p}_c and $\dot{\mathbf{p}}_c$. On flat ground, this nonlinearity is usually handled by assuming a constant CoM height, which leads to the well-known LIP model [1]. In order to allow for vertical movement of the CoM, a different choice is made here, which is to constrain the motion of the CoM to satisfy the relation $(\ddot{z}_c - g)/(z_c - z_z) = \eta^2$, where η is a constant parameter. The resulting dynamic model can be expressed in the form

$$\ddot{\mathbf{p}}_c = \eta^2(\mathbf{p}_c - \mathbf{p}_z) - \mathbf{g},\tag{A.2}$$

where $\mathbf{g} = (0 \ 0 \ g)^T$ is the gravity acceleration vector. This model features a LIP-like dynamic behavior along all three axes. The only difference with respect to a standard LIP is given by the gravity vector \mathbf{g} acting as a constant drift. This causes the system not to be in equilibrium when the CoM and ZMP coincide, but rather when they are displaced by \mathbf{g}/η^2 .

The choice of restricting the available trajectories to those resulting in a constant η allows to make the prediction model linear. If this restriction is removed, the model is referred to as Variable-Height Inverted Pendulum, which can be treated either as nonlinear or time-varying. This can allow for more general motions to be generated, e.g., running [46], at the cost of a slightly more complex architecture. For the present case, where only walking is considered, the simpler model is preferred.

In order to obtain smoother trajectories, model (A.2) is dynamically extended to have the derivative of the ZMP $\dot{\mathbf{p}}_z$ as the input. The gait generation scheme works over discrete time-steps of duration δ , over which the input $\dot{\mathbf{p}}_z$ is assumed to be constant, i.e., $\dot{\mathbf{p}}_z(t) = \dot{\mathbf{p}}_z^k$ for $t \in [t_k, t_{k+1})$. This prediction model is used to forecast the evolution of the system over a receding horizon window called the *control horizon*, spanning a time $T_c = C\delta$. The number of steps that are contained, either fully or partially, within this control horizon is denoted as F .

A.1.2 Stability Constraint

Model (A.2) has a positive eigenvalue η , reflecting the intrinsic instability of the humanoid dynamics. Given this instability, it is not sufficient to generate a gait such that the ZMP is inside the support region, because the associated CoM trajectory might be divergent, making the motion unrealizable by the humanoid. The role of the stability constraint is to enforce a condition on the unstable component of

the dynamics in order to guarantee that the CoM trajectory does not diverge with respect to the ZMP.

The unstable component of system (A.2) is highlighted by the coordinate $\mathbf{p}_u = \mathbf{p}_c + \dot{\mathbf{p}}_c/\eta$, also referred to as Divergent Component of Motion (DCM) or Capture Point (CP), that evolves according to the dynamics

$$\dot{\mathbf{p}}_u = \eta(\mathbf{p}_u - \mathbf{p}_z) - \frac{\mathbf{g}}{\eta}. \quad (\text{A.3})$$

Despite the instability, the evolution of the system is bounded if the following *stability condition* is satisfied

$$\mathbf{p}_u^k = \eta \int_{t_k}^{\infty} e^{-\eta(\tau-t_k)} \mathbf{p}_z(\tau) d\tau + \frac{\mathbf{g}}{\eta^2}, \quad (\text{A.4})$$

as stated by the following proposition.

Proposition 2 Consider system (A.2). If the ZMP velocity is bounded, $|\dot{x}_z| \leq v^{\max}$, $|\dot{y}_z| \leq v^{\max}$, $|\dot{z}_z| \leq v^{\max}$, for some $v^{\max} > 0$, and condition (A.4) is satisfied, then the following bound holds:

$$\frac{\mathbf{g}}{\eta^2} - \frac{v^{\max}}{\eta} \mathbf{1} \leq \mathbf{p}_c - \mathbf{p}_z \leq \frac{\mathbf{g}}{\eta^2} + \frac{v^{\max}}{\eta} \mathbf{1}, \quad (\text{A.5})$$

where $\mathbf{1}$ is a vector with all components equal to 1. Moreover, (A.5) implies that the system is internally stable, i.e., the CoM is bounded with respect to the ZMP.

Proof. See Appendix.

Condition (A.4) is non-causal as it requires knowledge of the future ZMP trajectory \mathbf{p}_z up to infinity. In order to derive a causal implementation, we split the integral at t_{k+C} . Of the two separate integrals that result, the first, over $[t_k, t_{k+C}]$, can be expressed in terms of the MPC decision variables. A value for the second integral, over $[t_{k+C}, \infty)$, can be obtained by conjecturing a ZMP trajectory using information coming from the footstep plan. This conjectured trajectory is called *anticipative tail* and is denoted with $\tilde{\mathbf{x}}_z$. In [20], the anticipative tail was used to prove recursive feasibility and stability of the MPC scheme.

The stability constraint is then written as

$$\eta \int_{t_k}^{t_{k+C}} e^{-\eta(\tau-t_k)} \mathbf{p}_z d\tau = \mathbf{p}_u^k - \tilde{\mathbf{c}}^k - \frac{\mathbf{g}}{\eta^2}. \quad (\text{A.6})$$

where $\tilde{\mathbf{c}}^k$ is given by

$$\tilde{\mathbf{c}}^k = \eta \int_{t_{k+C}}^{\infty} e^{-\eta(\tau-t_k)} \tilde{\mathbf{p}}_z d\tau. \quad (\text{A.7})$$

Note that in [20] we considered the footstep plan to be available over a receding window called the *preview horizon*. Here there is no need to make such an assumption, as the footstep plan is provided in its entirety, and once the goal is reached the robot comes to a complete stop.

Enforcing constraint (A.6) allows, similarly to what stated in Prop. 2, to bound the displacement between CoM and ZMP. In fact, the value of the bound is almost identical in most practical situation, especially in view of the fact that the preview horizon is unlimited because the plan is completely known. Because of this fact, we will assume in the following that Prop. 2 is valid as stated, even though a small numerical correction should be applied to make up for the difference between the stability condition and the stability constraint.

A.1.3 ZMP Velocity Constraint

This constraint imposes a limit on how fast the ZMP can move, i.e.,

$$|\dot{x}_z| \leq v^{\max}, \quad |\dot{y}_z| \leq v^{\max}, \quad |\dot{z}_z| \leq v^{\max} \quad (\text{A.8})$$

Enforcing such limit allows to indirectly control the maximum CoM/ZMP displacement, by using the result of Prop. 2. This will be useful when defining the ZMP position constraint, as will be made clear in the following paragraphs.

A.1.4 ZMP Position Constraint

As already noted, the humanoid is balanced as long as the ZMP is inside the pyramid \mathcal{Z} , which is a nonlinear condition due to the vertex of the pyramid being at the CoM (Fig. A.1). To preserve linearity we consider a smaller allowed region for the ZMP, consisting in a box of fixed size with changing center and orientation. We refer to this as the *moving box*¹, and we will prove that it conservatively approximates the support region, meaning that it is always contained inside the pyramid \mathcal{Z} .

The center \mathbf{p}_{mc} and orientation θ_{mc} of the moving box are taken to be consistent with the pose of footstep \mathbf{f}^j during the j -th single support phase. In the following double support phase they will gradually slide in order to reach the pose of the next footstep \mathbf{f}^{j+1} , with a linear² timing law. At each time t , the center of the moving box \mathbf{p}_{mc} is expressed as

$$\mathbf{p}_{\text{mc}}(t) = \begin{cases} \mathbf{p}^j & t \in [t_s^j, t_s^j + T_{\text{ss}}^j) \\ (1 - \alpha^j(t))\mathbf{p}^j + \alpha^j(t)\mathbf{p}^{j+1} & t \in [t_s^j + T_{\text{ss}}^j, t_s^{j+1}) \end{cases} \quad (\text{A.9})$$

where $j = 0, \dots, F$ is a index over the footsteps within the control horizon, and $\alpha^j(t) = (t - t_s^j - T_{\text{ss}}^j)/T_{\text{ds}}$ denotes the time elapsed since the start of the double support phase, expressed as a fraction of the duration of the double support phase itself. The orientation of the moving box θ_{mc} can be similarly expressed as

$$\theta_{\text{mc}}(t) = \begin{cases} \theta^j & t \in [t_s^j, t_s^j + T_{\text{ss}}^j) \\ \text{anglin}(\theta^j, \theta^{j+1}, \alpha^j(t)) & t \in [t_s^j + T_{\text{ss}}^j, t_s^{j+1}) \end{cases} \quad (\text{A.10})$$

¹Approximating the pyramidal region \mathcal{Z} with a box might seem overly conservative. However, we argue that the neglected portion of the pyramid region is not crucial here, because large displacements of the ZMP in the z direction would only be required to generate large vertical accelerations, which are not necessary in the considered setting (walking in a world of stairs). Clearly, less conservative approximations can still be envisaged and used for generating more dynamic motions.

²The timing law can be arbitrarily chosen as long as it leads the moving box from one footstep to the next within the duration of the double support phase.

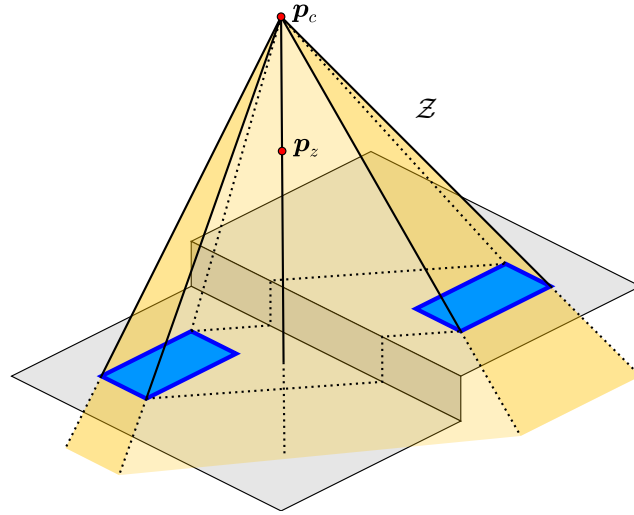


Figure A.1. Balance condition in 3D: the ZMP must lie inside the yellow pyramid.

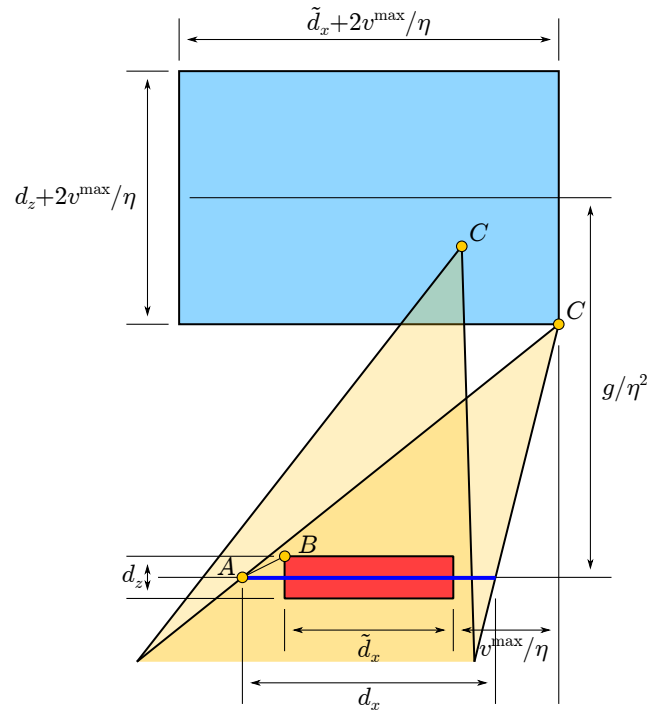


Figure A.2. The red rectangle represents a section of the moving box in the x - z plane. This region is fully contained inside the yellow pyramid as long as the CoM belongs to the blue region. Here, two scenarios are considered: one in which the CoM is well within the blue region, and a worst-case scenario in which the CoM is in a lower vertex of the blue region.

where $j = 0, \dots, F$, and anglin is a function³ that computes a linear combination of angles in such a way to correctly account for wrapping around $\pm\pi$.

The ZMP position constraint is expressed as

$$-\tilde{\mathbf{d}}/2 \leq \mathbf{R}_{k+i}^T(\mathbf{p}_z^{k+i} - \mathbf{p}_{\text{mc}}^{k+i}) \leq \tilde{\mathbf{d}}/2 \quad (\text{A.11})$$

where \mathbf{p}_z^{k+i} and $\mathbf{p}_{\text{mc}}^{k+i}$ respectively denote the ZMP and the center of the moving box sampled at time t_{k+i} , $\tilde{\mathbf{d}} = (\tilde{d}_x, \tilde{d}_y, d_z)^T$ is a vector collecting the dimensions of the moving box along all three axes, and \mathbf{R}_{k+i} is the rotation matrix associated with θ_{mc}^{k+i} .

The size of the moving box $\tilde{\mathbf{d}} = (\tilde{d}_x, \tilde{d}_y, d_z)^T$ is determined in such a way to always be contained inside the pyramid \mathcal{Z} , as expressed by the following proposition.

Proposition 3 *Assume the stability constraint (A.6) and the ZMP velocity constraint (A.8) are enforced. If v^{\max} is chosen in such a way that*

$$v^{\max} \leq \min\{v_y^{\max}, v_x^{\max}\}, \quad (\text{A.12})$$

where v_x^{\max} and v_y^{\max} are given by the following compact expression

$$v_{x,y}^{\max} = \eta \left(g/\eta^2 - d_{x,y} \frac{d_z}{d_{x,y} - \tilde{d}_{x,y}} \right) \left(1 + \frac{d_z}{d_{x,y} - \tilde{d}_{x,y}} \right)^{-1}, \quad (\text{A.13})$$

with d_x and d_y denoting the size of the actual footprint, then the moving box is always contained in the pyramid \mathcal{Z} .

Proof. Consider the geometric construction in Fig. A.2. This construction shows a projection of the pyramid \mathcal{Z} in the x - z plane during a single support phase. The red area represents a cross section of the moving box, with dimensions \tilde{d}_x and d_z . The blue area represents the region where the CoM can be found, given the CoM/ZMP bounds (A.5). In the figure two different possibilities are depicted for the CoM position (identified by the point C). Among them, consider the worst-case scenario, in which the CoM is in the bottom-right corner of the blue region⁴. A condition for which the red region is always fully contained inside \mathcal{Z} can be found by imposing that the slope of the segment AB is less than the slope of the segment AC , i.e.,

$$\frac{d_z/2}{d_x/2 - \tilde{d}_x/2} \leq \frac{g/\eta^2 - d_z/2 - v_x^{\max}/\eta}{d_x/2 + \tilde{d}_x/2 + v_x^{\max}/\eta}, \quad (\text{A.14})$$

which, after simple manipulations, leads to (A.13). During double support phases the construction of Fig. A.2 is not accurate anymore, as the pyramid \mathcal{Z} is much

³For two generic angles θ_a and θ_b , linearly combined with a weight α , the function anglin can be defined as

$$\begin{aligned} \text{anglin}(\theta_a, \theta_b, \alpha) &= \text{atan2}(\sin((1 - \alpha)\theta_a) + \sin(\alpha\theta_b), \\ &\quad \cos((1 - \alpha)\theta_a) + \cos(\alpha\theta_b)). \end{aligned}$$

Note that this definition is meaningless when the two angles are separated by exactly π , but this can never occur as the angle between consecutive footsteps is limited by requirement R2.

⁴An equivalent symmetrical scenario would occur if the CoM were in the bottom-left corner.

larger than the one represented. However, it is not necessary to repeat the reasoning, as a smaller pyramid, analogous to that shown in Fig. A.2, can always be constructed and will always be contained inside \mathcal{Z} . The last step is to repeat the construction in the y - z plane in order to find v_y^{\max} , which proves the thesis. ■

A.1.5 QP Problem

At a generic time t_k , IS-MPC solves the following QP problem

$$\left\{ \begin{array}{l} \min_{\dot{\mathbf{p}}_z^k, \dots, \dot{\mathbf{p}}_z^{k+C-1}} \sum_{i=0}^{C-1} \left(\|\dot{\mathbf{p}}_z^{k+i}\|^2 + \beta \|\mathbf{p}_z^{k+i} - \mathbf{p}_{\text{mc}}^{k+i}\|^2 \right) \\ \text{subject to:} \\ \bullet \text{ stability constraint (A.6)} \\ \bullet \text{ ZMP velocity constraint (A.8)} \\ \bullet \text{ ZMP position constraint (A.11)} \end{array} \right.$$

The cost function minimizes the decision variables (ZMP derivative) as a regularization term, and attempts to bring the ZMP close to the center of the moving box, which is typically beneficial as it produces a more robust walking pattern. β is a weight on the second term.

In typical MPC fashion, the first sample of the ZMP velocity $\dot{\mathbf{p}}_z^k$ is used to integrate the 3D LIP dynamics (A.2). The resulting CoM trajectory \mathbf{p}_c is sent, together with the swing foot trajectory generated by the footstep planner and sampled at time t_k , to the kinematic controller.

A.1.6 Proof of Prop. 2

Starting from the initial condition $\mathbf{p}_u(t_k)$ described by (A.4), the unstable coordinate \mathbf{p}_u evolves as

$$\mathbf{p}_u(t) = \eta \int_t^\infty e^{-\eta(\tau-t)} \mathbf{p}_z(\tau) d\tau + \frac{\mathbf{g}}{\eta^2}. \quad (\text{A.15})$$

Integrating A.15 by parts gives

$$\mathbf{p}_u(t) - \mathbf{p}_z(t) - \frac{\mathbf{g}}{\eta^2} = \int_t^\infty e^{-\eta(\tau-t)} \dot{\mathbf{p}}_z d\tau. \quad (\text{A.16})$$

Since by hypothesis the ZMP velocity $\dot{\mathbf{p}}_z$ is component-wise bounded, i.e., $|\dot{x}_z| \leq v^{\max}$, $|\dot{y}_z| \leq v^{\max}$, $|\dot{z}_z| \leq v^{\max}$, then the following upper bound is obtained

$$\mathbf{p}_u(t) - \mathbf{p}_z(t) - \frac{\mathbf{g}}{\eta^2} \leq v^{\max} \mathbf{1} \int_t^\infty e^{-\eta(\tau-t)} d\tau,$$

along with a similar lower bound. The two bounds can be combined in the following expression

$$-\frac{v^{\max}}{\eta} \mathbf{1} \leq \mathbf{p}_u(t) - \mathbf{p}_z(t) - \frac{\mathbf{g}}{\eta^2} \leq \frac{v^{\max}}{\eta} \mathbf{1}. \quad (\text{A.17})$$

Define now the coordinate $\mathbf{p}_s = \mathbf{p}_c - \dot{\mathbf{p}}_c/\eta$. This coordinate pertains to the stable eigenvalue of system (A.2), and its dynamics can be expressed as

$$\dot{\mathbf{p}}_s = \eta(-\mathbf{p}_s + \mathbf{p}_z) + \frac{\mathbf{g}}{\eta}.$$

Starting from an initial time t_0 , the coordinate \mathbf{p}_s evolves as

$$\mathbf{p}_s(t) = \mathbf{p}_s(t_0)e^{-\eta(t-t_0)} + \eta \int_{t_0}^t e^{-\eta(t-\tau)} \left(\mathbf{p}_z(\tau) + \frac{\mathbf{g}}{\eta^2} \right) d\tau.$$

Similarly to \mathbf{p}_u , the above expression can manipulated using integration by parts, and the resulting integral can be bounded using the hypothesis on the ZMP velocity. The resulting expression is

$$-\frac{v^{\max}}{\eta} \mathbf{1} + \mathbf{s}_0 \leq \mathbf{p}_s(t) - \mathbf{p}_z(t) - \frac{\mathbf{g}}{\eta^2} \leq \frac{v^{\max}}{\eta} \mathbf{1} + \mathbf{s}_0,$$

where $\mathbf{s}_0 = \mathbf{p}_s(t_0) - \mathbf{p}_z(t_0) - \mathbf{g}/\eta^2$. Since at t_0 the robot is typically in static equilibrium, corresponding to $\mathbf{p}_c(t_0) = \mathbf{p}_z(t_0) + \mathbf{g}/\eta^2$ and $\dot{\mathbf{p}}_c(t_0) = 0$, then $\mathbf{s}_0 = 0$. This leads to

$$-\frac{v^{\max}}{\eta} \mathbf{1} \leq \mathbf{p}_s(t) - \mathbf{p}_z(t) - \frac{\mathbf{g}}{\eta^2} \leq \frac{v^{\max}}{\eta} \mathbf{1}. \quad (\text{A.18})$$

By noting that $2\mathbf{p}_c = \mathbf{p}_u + \mathbf{p}_s$, combining eqs. (A.17) and (A.18) proves the thesis.

Appendix B

Real-time nonlinear model predictive control

Todo.

Bibliography

- [1] S. Kajita, F. Kanehiro, K. Kaneko, K. Fujiwara, K. Harada, K. Yokoi, and H. Hirukawa. Biped walking pattern generation by using preview control of zero-moment point. In *2003 IEEE Int. Conf. on Robotics and Automation*, pages 1620–1626, 2003.
- [2] Tomomichi Sugihara, Kenta Imanishi, Takanobu Yamamoto, and Stéphane Caron. 3D biped locomotion control including seamless transition between walking and running via 3D ZMP manipulation. In *2021 IEEE Int. Conf. on Robotics and Automation*, pages 6258–6263, 2021.
- [3] Stéphane Caron, Adrien Escande, Leonardo Lanari, and Bastien Mallein. Capturability-based pattern generation for walking with variable height. *IEEE Transactions on Robotics*, 36(2):517–536, 2019.
- [4] Alessio Zamparelli, Nicola Scianca, Leonardo Lanari, and Giuseppe Oriolo. Humanoid gait generation on uneven ground using intrinsically stable MPC. *IFAC-PapersOnLine*, 51:393–398, 2018.
- [5] Paolo Ferrari, Nicola Scianca, Leonardo Lanari, and Giuseppe Oriolo. An integrated motion planner/controller for humanoid robots on uneven ground. In *18th European Control Conference*, pages 1598–1603, 2019.
- [6] A. Ibanez, P. Bidaud, and V. Padois. Emergence of humanoid walking behaviors from Mixed-integer Model Predictive Control. In *2014 IEEE/RSJ Int. Conf. on Intelligent Robots and Systems*, pages 4014–4021, 2014.
- [7] Young-Dae Hong, Ye-Hoon Kim, Ji-Hyeong Han, Jeong-Ki Yoo, and Jong-Hwan Kim. Evolutionary Multiobjective Footstep Planning for Humanoid Robots. *IEEE Transactions on Systems, Man, and Cybernetics, Part C (Applications and Reviews)*, 41(4):520–532, 2011.
- [8] Mohammadreza Kasaei, Ali Ahmadi, Nuno Lau, and Artur Pereira. A modular framework to generate robust biped locomotion: from planning to control. *SN Applied Sciences*, 3:1–18, 2021.
- [9] Robin Deits and Russ Tedrake. Footstep planning on uneven terrain with mixed-integer convex optimization. In *2014 IEEE-RAS Int. Conf. on Humanoid Robots*, pages 279–286, 2014.

- [10] Daeun Song, Pierre Fernbach, Thomas Flayols, Andrea Del Prete, Nicolas Mansard, Steve Tonneau, and Young J. Kim. Solving Footstep Planning as a Feasibility Problem Using L1-Norm Minimization. *IEEE Robotics and Automation Letters*, 6:5961–5968, 2021.
- [11] Robert J. Griffin, Georg Wiedebach, Stephen McCrary, Sylvain Bertrand, Inho Lee, and Jerry Pratt. Footstep Planning for Autonomous Walking Over Rough Terrain. In *2019 IEEE Int. Conf. on Robotics and Automation*, pages 9–16, 2019.
- [12] Hong Liu, Qing Sun, and Tianwei Zhang. Hierarchical RRT for Humanoid Robot Footstep Planning with Multiple Constraints in Complex Environments. In *2012 IEEE/RSJ Int. Conf. on Intelligent Robots and Systems*, pages 3187–3194, 2012.
- [13] Kei Okada, Takashi Ogura, Atsushi Haneda, and Masayuki Inaba. Autonomous 3D walking system for a humanoid robot based on visual step recognition and 3D foot step planner. In *2005 IEEE Int. Conf. on Robotics and Automation*, pages 623–628, 2005.
- [14] Joel Chestnutt, Yutaka Takaoka, Keisuke Suga, Koichi Nishiwaki, James Kuffner, and Satoshi Kagami. Biped navigation in rough environments using on-board sensing. In *2009 IEEE/RSJ Int. Conf. on Intelligent Robots and Systems*, pages 3543–3548, 2009.
- [15] Maurice F. Fallon, Pat Marion, Robin Deits, and Thomas Whelan. Continuous humanoid locomotion over uneven terrain using stereo fusion. In *2015 IEEE-RAS Int. Conf. on Humanoid Robots*, pages 881–888, 2015.
- [16] Daniel Maier, Christian Lutz, and Maren Bennewitz. Integrated perception, mapping, and footstep planning for humanoid navigation among 3d obstacles. In *2013 IEEE/RSJ Int. Conf. on Intelligent Robots and Systems*, pages 2658–2664, 2013.
- [17] Alexander Stumpf, Stefan Kohlbrecher, David C Conner, and Oskar von Stryk. Supervised footstep planning for humanoid robots in rough terrain tasks using a black box walking controller. In *2014 IEEE-RAS Int. Conf. on Humanoid Robots*, pages 287–294, 2014.
- [18] Philipp Karkowski, Stefan Oßwald, and Maren Bennewitz. Real-time footstep planning in 3D environments. In *2016 IEEE-RAS Int. Conf. on Humanoid Robots*, pages 69–74, 2016.
- [19] Takanobu Yamamoto and Tomomichi Sugihara. Responsive navigation of a biped robot that takes into account terrain, foot-reachability and capturability. *Advanced Robotics*, 35(8):516–530, 2021.
- [20] Nicola Scianca, Daniele De Simone, Leonardo Lanari, and Giuseppe Oriolo. MPC for humanoid gait generation: Stability and feasibility. *IEEE Transactions on Robotics*, 36(4):1171–1178, 2020.

- [21] Wolfram Burgard, Martial Hebert, and Maren Bennewitz. World Modeling. In *Springer handbook of robotics*, pages 1135–1152. Springer, 2016.
- [22] Adrien Escande, Nicolas Mansard, and Pierre-Brice Wieber. Hierarchical quadratic programming: Fast online humanoid-robot motion generation. *Int. J. of Robotics Research*, 33(7):1006–1028, 2014.
- [23] Sertac Karaman and Emilio Frazzoli. Sampling-based algorithms for optimal motion planning. *Int. J. of Robotics Research*, 30(7):846–894, 2011.
- [24] Anna Yershova and Steven M LaValle. Improving motion-planning algorithms by efficient nearest-neighbor searching. *IEEE Transactions on Robotics*, 23(1):151–157, 2007.
- [25] Mathieu Labb  and Fran ois Michaud. RTAB-Map as an open-source lidar and visual simultaneous localization and mapping library for large-scale and long-term online operation. *Journal of Field Robotics*, 36(2):416–446, 2019.
- [26] Basile G. Rabbat and Henry G. Russell. Friction coefficient of steel on concrete or grout. *Journal of Structural Engineering*, 111:505–515, 1985.
- [27] P ter Fankhauser, Michael Bloesch, and Marco Hutter. Probabilistic Terrain Mapping for Mobile Robots with Uncertain Localization. *IEEE Robotics and Automation Letters*, 3(4):3019–3026, 2018.
- [28] Fran ois Chaumette, Seth Hutchinson, and Peter Corke. Visual servoing. In *Springer Handbook of Robotics*, pages 841–866. Springer, 2016.
- [29] A. Herdt, N. Perrin, and P. B. Wieber. Walking without thinking about it. In *2010 IEEE/RSJ Int. Conf. on Intelligent Robots and Systems*, pages 190–195, 2010.
- [30] Marcos R. O. A. Maximo and Rubens J. M. Afonso. Mixed-integer quadratic programming for automatic walking footstep placement, duration, and rotation. *Optimal Control Applications and Methods*, 41(6):1928–1963, 2020.
- [31] N stor Boh rquez and Pierre-Brice Wieber. Adaptive step duration in biped walking: A robust approach to nonlinear constraints. In *17th IEEE-RAS Int. Conf. on Humanoid Robots*, pages 724–729, 2017.
- [32] St phane Caron and Quang-Cuong Pham. When to make a step? tackling the timing problem in multi-contact locomotion by topp-mpc. In *17th IEEE-RAS Int. Conf. on Humanoid Robots*, pages 522–528, 2017.
- [33] Aurelien Ibanez, Philippe Bidaud, and Vincent Padois. Emergence of humanoid walking behaviors from mixed-integer model predictive control. In *2014 IEEE/RSJ Int. Conf. on Intelligent Robots and Systems*, pages 4014–4021, 2014.
- [34] Filippo M. Smaldone, Nicola Scianca, Leonardo Lanari, and Giuseppe Oriolo. Feasibility-driven step timing adaptation for robust MPC-based gait generation in humanoids. *IEEE Robotics and Automation Letters*, 6(2):1582–1589, 2021.

- [35] Majid Khadiv, Alexander Herzog, S. Ali. A. Moosavian, and Ludovic Righetti. Walking control based on step timing adaptation. *IEEE IEEE Trans. on Robotics*, 36(3):629–643, 2020.
- [36] M. Naveau, M. Kudruss, O. Stasse, C. Kirches, K. Mombaur, and P. Souères. A reactive walking pattern generator based on nonlinear model predictive control. *IEEE Robotics and Automation Letters*, 2(1):10–17, 2017.
- [37] Néstor Bohórquez and Pierre-Brice Wieber. Adaptive step rotation in biped walking. In *2018 IEEE/RSJ Int. Conf. on Intelligent Robots and Systems*, pages 720–725, 2018.
- [38] Bernardo Aceituno-Cabezas, Carlos Mastalli, Hongkai Dai, Michele Focchi, Andreea Radulescu, Darwin G. Caldwell, José Cappelletto, Juan C. Grieco, Gerardo Fernández-López, and Claudio Semini. Simultaneous contact, gait, and motion planning for robust multilegged locomotion via mixed-integer convex optimization. *IEEE Robotics and Automation Letters*, 3(3):2531–2538, 2018.
- [39] Andrew S Habib, Filippo M Smaldone, Nicola Scianca, Leonardo Lanari, and Giuseppe Oriolo. Handling non-convex constraints in mpc-based humanoid gait generation. In *2022 IEEE/RSJ Int. Conf. on Intelligent Robots and Systems*, pages 13167–13173, 2022.
- [40] Jiatao Ding, Xiaohui Xiao, and Nikos Tsagarakis. Nonlinear optimization of step duration and step location. In *2019 IEEE/RSJ Int. Conf. on Intelligent Robots and Systems*, pages 2259–2265, 2019.
- [41] Michele Cipriano, Paolo Ferrari, Nicola Scianca, Leonardo Lanari, and Giuseppe Oriolo. Humanoid motion generation in a world of stairs. *Robotics and Autonomous Systems*, 168:104495, 2023.
- [42] J. Englsberger, C. Ott, and A. Albu-Schäffer. Three-dimensional bipedal walking control based on divergent component of motion. *IEEE Transactions on Robotics*, 31(2):355–368, 2015.
- [43] J. Pratt, J. Carff, S. Drakunov, and A. Goswami. Capture point: A step toward humanoid push recovery. In *6th IEEE-RAS Int. Conf. on Humanoid Robots*, pages 200–207, 2006.
- [44] T. Sugihara, Y. Nakamura, and H. Inoue. Real-time humanoid motion generation through ZMP manipulation based on inverted pendulum control. In *2002 IEEE Int. Conf. on Robotics and Automation*, volume 2, pages 1404–1409, 2002.
- [45] Rubens J.M. Afonso, Marcos R. O. A. Maximo, and Roberto K.H. Galvão. Task allocation and trajectory planning for multiple agents in the presence of obstacle and connectivity constraints with mixed-integer linear programming. *Int. Journal of Robust and Nonlinear Control*, 30(14):5464–5491, 2020.
- [46] Filippo M Smaldone, Nicola Scianca, Leonardo Lanari, and Giuseppe Oriolo. From walking to running: 3D humanoid gait generation via MPC. *Frontiers in Robotics and AI*, 9, 2022.